A model-measurements comparison of atmospheric forcing and surface fluxes of the Baltic Sea

Diplomarbeit

von

Claudia Rudolph

Mathematisch-Naturwissenschaftliche Falkultät
der Christian-Albrechts-Universität zu Kiel
Erstellt am Leibniz-Institut für Meereswissenschaften
Forschungsbereich 1
-Maritime Meteorologie-

Kiel
2006

Chapter 1

Introduction

The interaction between atmosphere and ocean is largely driven by the energy and water cycle which in turn is determined by the development and energetics of clouds, water vapor and precipitation. Forming these cycles within and among the components of the climate system, water in all of its three phases causes much of the complexity and variability of weather and climate. The quantification of the water and energy budget of the Baltic Sea area is the central aim of the BALTEX (Baltic Sea Experiment) research program (BALTEX, 1995, 2004, 2006). Furthermore, the correct simulation of the energy and water budget is an important requirement for the quality of numerical models, which later can be used for studies of extreme events and climate change in the Baltic area. On the other hand, improved knowledge of energy and water budgets can only be obtained by sophisticated numerical models, including data assimilation. Thus, for a better understanding of the energy and water cycles in the Baltic area, a more detailed validation of model components and a more extensive use of already available observations and satellite measurements are required. The detailed evaluation must therefore include not only the standard parameters but also fluxes; in other words, it will involve a detailed analysis of coupling mechanisms and forcing functions.

Generally speaking, models for the Baltic Sea area show that most of the characteristics of the Baltic Sea and the overlying atmosphere can be described realistically (e.g. Schrum and Backhaus 1999, Omstedt and Rutgersson 2000, Gustafsson 2000a,b, Lehmann and Hinrichsen 2000b, Jacob 2001, Rummukainen et al. 2001, Meier & Döscher 2002). However, the representation of physical exchange processes between ocean and atmosphere still suffers from inadequately resolved processes. Modelling large and small scales requires a better knowledge of surface

fluxes, which are difficult to measure directly on these scales. In general, vertical fluxes of momentum, sensible and latent heat are parameterised by bulk aerodynamic formulas. However, for Baltic Sea modelling purposes, no preference for a specific form of these formulas can be found in the literature. Thus, comparing estimations of the energy and water budget from different models that employ different parameterisations of the exchange fluxes may well exhibit greater differences. How can the reliability of the models be increased and how can uncertainties be reduced?

Atmosphere-ocean or land-atmosphere fluxes are one key-process in controlling the behavior of different models. Uncoupled versions of sophisticated models (e.g. atmosphere only, sea ice-ocean only) often perform even better than in the coupled mode. This is a clear indicator of the important role of fluxes. In an atmosphere model the ocean surface temperatures and the extent of sea-ice are prescribed; such a model is thus controlled by ocean parameters. In a sea ice-ocean model, surface fluxes between atmosphere and ocean drive the ocean model.

Comprehensive data sets suitable to validating coupled model systems, and hence, the corresponding parameterisations of fluxes are few in number. However, within the BALTIMOS project, eight field campaigns over the open and ice-covered Baltic Sea have were conducted during the period 1998-2001 (Brümmer et al. 2003). The observations focused mainly on:

- the atmospheric boundary layer structure and processes, and the air-sea-ice interaction over areas with inhomogeneous sea-ice cover
- the atmospheric boundary layer structure over open water under different synoptic conditions such as cold- and warm-air advection and frontal passages.

Gathered systematically during all four seasons and over open water and sea ice of the Baltic Sea, these data sets are ideally suited for validation of coupled model systems. In Brümmer et al. (2003) explicitly encouraged potential users to use such data sets.

The aim of the work is to allow a carefully detailed comparison of extracted model data with these data sets and to carefully evaluate the atmospheric forcing, corresponding surface fluxes and surface response of the three-dimensional coupled sea ice-ocean model BSIOM (Lehmann & Hinrichsen 2000a, 2002).

Further, a statistical comparison of meteorological quantities, radiation fluxes and heat fluxes of the BALTIMOS experiments with calculated model data were carried out, as well as long time periods of Kiel institute and Kiel lighthouse for the years 1998, 2000 and 2001 were utilised to evaluate statistically the atmospheric forcing of the coupled sea ice-ocean model BSIOM.

The diploma thesis is organised as follows: Section 2 includes some information about the characteristics of the Baltic Sea. Section 3 describes the Baltic Sea Ice-Ocean Model (BSIOM) and gives the corresponding parameterisations of the fluxes. Section 4 comprises the interactions of ocean and atmosphere, and section 5 describes the parameterisation of turbulent processes. Section 6 compares meteorological conditions, radiation fluxes and heat fluxes with observations. Section 7 comprises a statistical comparison; it is followed in Section 8 by a discussion. The thesis ends with a summary and conclusions.

Chapter 2

Baltic Sea

The Baltic Sea (Figure 1) covers an area of approximately 422,000 km^2. The whole region around the Baltic Sea is characterized by strong contrasts in vegetation, geology and climate. Many of lakes and crystalline rocks of the basement affect the natural scenery in the North, whereas in the South more glacial sediments and sandy or loamy soil are present. The vegetation is characterized by great boreal forest areas in the North and by agrarian areas in the South.

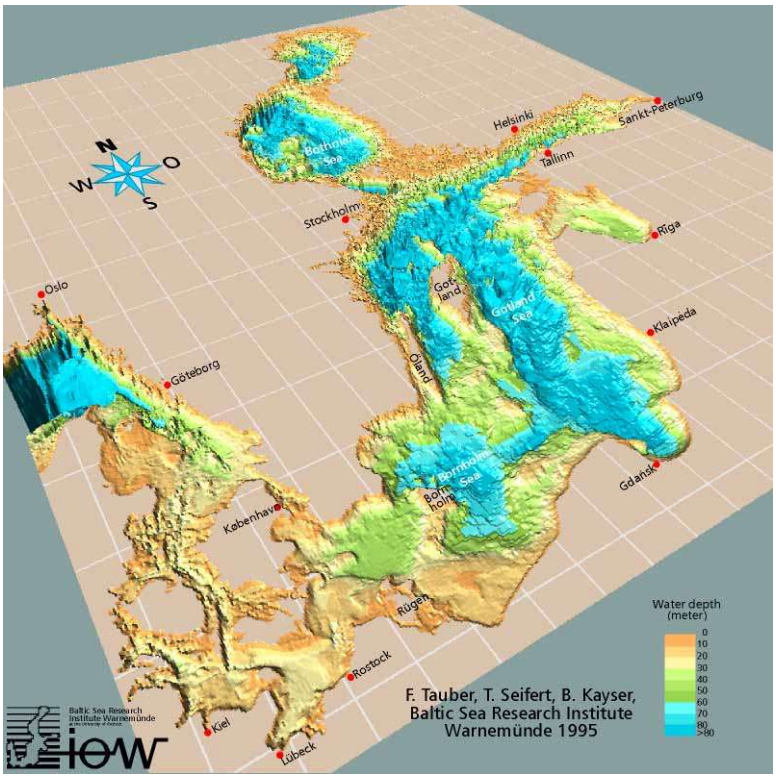

Figure 1. Topography of the Baltic Sea

The Baltic Sea is a unique brackish semi-enclosed sea, which is connected to the North Sea through the narrow and shallow Danish Straits, with an extension of 1700 km in the north-south direction. The southern parts belong to Central Europe and the northern area lies beyond the Arctic Circle. The Baltic Sea is a shallow water basin located on one tectonic plate, with only a mean depth of 50 meters. The greatest depth is Landsort Deep with 459 meters located in the western Gotland Basin.

The Baltic Sea can be described as a large estuary with an upper layer of brackish water and a lower layer of saline water. The passage to the North Sea with its shallow and narrow straits restricts the water mass exchange between the North Sea and the Baltic Sea. The outflow of brackish Baltic Sea water at the surface and a compensating inflow of haline water near the bottom establish a haline stratification in the Belt Sea most time of the year (Wyrtki 1953). The inflow of North Sea water is sporadic and dependends on weather situations, so that under strong west wind conditions, the stratification is broken up by mixing and a huge amount of highly saline water can penetrate into the Baltic Sea. After passing the Drodgen and Darss sill the highly saline water sinks down and follows the bottom topography. Also, the haline stratification is determined by the huge fresh water contribution from the rivers and the net effect of precipitation minus evaporation. The water above the permanent halocline can directly interact (heat exchange) with the atmosphere whereas the water below the halocline is insulated due to strong stratification which restricts an effective convective exchange across the halocline. Thus any changes of fresh water and salt fluxes will have impact on the haline stratification and in turn will affect the heat budget of the Baltic Sea. The thickness of the brackish water mass above the halocline thus influences the development of the sea surface temperate and sea ice during winter, which both affect the interaction with the atmosphere (Lehmann & Hinrichsen 2002). During spring and summer a seasonal thermocline develops which is eroded in autumn by turbulent mixing due to strong wind events (Krauss 1981).

Climatological conditions of the Baltic Sea area reach from mild and moist climate in the South to subarctic climate in the North, which is a principal reason for the large inter-annual variations in the winter weather. The weather is predominately affected by location, intensity and flexion of the westerly drift. Generally, the prevailing conditions are affected by local and regional large scale weather systems. On average, during winter the Baltic Sea freezes with an ice extension of about 200,000 km², which is half of the total area of the Baltic Sea (Figure 2). Normally, the sea ice season lasts from October/November to May/June. The annual maximum ice extend occurs between January and March. Thickness and duration shows large

inter-annual variability, for example during extremely mild winters the maximum extent is well below 100,000 km², which is seen in Figure 2 (hatched area), because predominately westerly winds transport warm and wet air masses to the Baltic area, the minimum for example in 1989 were only 52,000 km² (Seinä et al., 1991). On the contrary, when continental weather systems prevail, the ice extent becomes large, so that in extreme ice winters, almost the whole Baltic Sea may become frozen (dashed area). The extent and thickness of sea ice in the Baltic Sea are highly sensitive to climate variability and change.

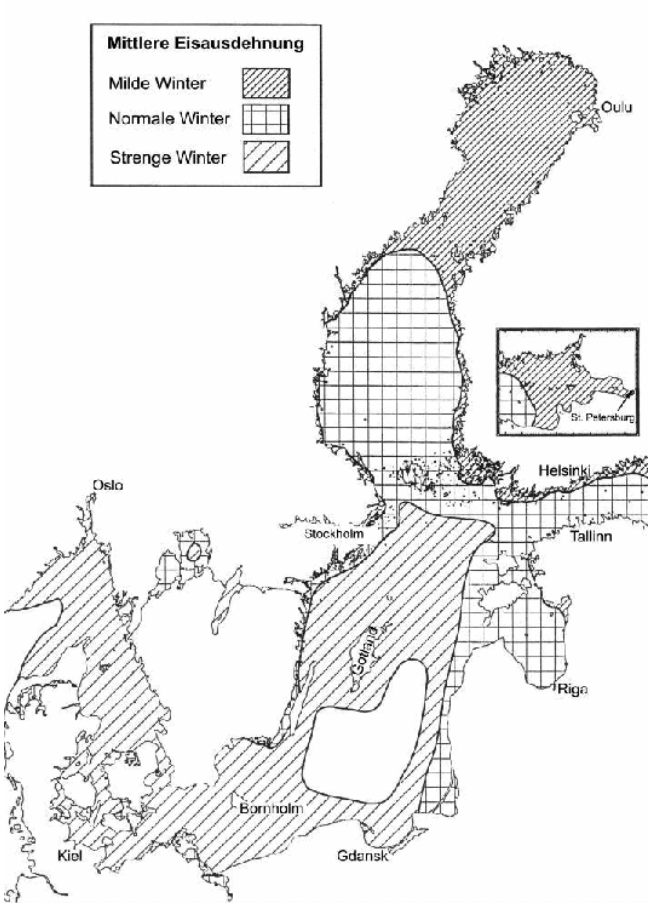

Figure 2. Mean ice extent of the Baltic Sea. Hatched area for mild winter, chequered area for normal winter and dashed area for severe winter.

Chapter 3

Baltic Sea Model

The numerical model, used in this study, is a general three-dimensional coupled sea-ice-ocean model of the Baltic Sea (BSIOM; Lehmann & Hinrichsen 2000a, 2002). The horizontal resolution of the coupled sea-ice ocean model is 5 km (eddies permitting), and in the vertical 60 levels are specified, which enable the upper 100 m to be resolved with levels of 3 m thickness. The model domain comprises the Baltic Sea, including the Kattegat and Skagerrak. At the western boundary, a simplified North Sea basin is connected to the Skagerrak to take up sea level elevations and to provide characteristic North Sea water masses which result from different forcing conditions (Lehmann 1995, Novotny et al. 2005). At the western boundary of the simplified North Sea (4°E), the sea level is adjusted to a constant reference value, which has been determined from the sea level inclination calculated from the initial density distribution. With respect to the reference level, volume is supplied/extracted from the North Sea in case of in/outflow conditions. The salinity in the North Sea basin is relaxed to a climatology. Thus, sea level changes in the Skagerrak are determined by the atmospheric forcing acting on the total model domain including the area of the simplified North Sea and river runoff supplied to the Baltic Sea and the Kattegat. Sea level changes propagating into the North Sea from Atlantic and tides are not considered.

The coupled sea-ice-ocean model is forced by realistic atmospheric conditions taken from the Swedish Meteorological and Hydrological Institute's (SMHI, Norrköping, Sweden) meteorological database (Lars Meuller, pers. comm.) which covers the whole Baltic drainage basin on a regular grid of 1 x 1° with a temporal increment of 3 hours. The database consists of synoptic measurements interpolated on the regular grid by using a two-dimensional univariate optimum interpolation scheme. This database, which for modelling purposes is further interpolated onto the model grid,

includes surface pressure, precipitation, cloudiness, air temperature and water vapour mixing ratio at 2 m height and the geostrophic wind. Wind speed and direction at 10 m height are calculated from geostrophic winds with respect to different degrees of roughness on the open sea and in coastal waters (Bumke et al. 1998).

The calculation of the ocean-atmosphere energy exchange is based on the following simplified surface heat balance equation for open and ice-covered water:

$$Q_{net} = H + E + (1 - \alpha)S_o(o) + Lw(o) - Lw(u), \quad (3.1)$$

where Q_{net} is the net heat flux entering the oceanic mixed layer, H and E are the sensible and latent heat fluxes, respectively, $(1 - \alpha)S_o(o)$ is the absorbed short-wave radiation, $Lw(o)$ is the incoming atmospheric long-wave radiation and $Lw(u)$ is the long-wave radiation leaving the sea surface.

Surface fluxes are calculated from atmospheric data and modelled SSTs with the aid of bulk aerodynamic formulas. Wind stress on the ocean surface is calculated from the 10 m wind, with the drag coefficient according to Large and Pond (1981). The drag coefficient over sea-ice is chosen to be constant (Joffre, 1982). The combined wind stress on ice and ocean surfaces is formulated as:

$$\tau = \rho U_{10}^2((1 - A)C_{dao} + AC_{dai}). \quad (3.2)$$

Here, $C_{dai} = 1.5\text{x}10^{-3}$ and C_{dao} - the drag coefficients for the atmosphere-ice and atmosphere-ocean interface, ρ - the air density, A - the ice fraction and U_{10} - the wind speed at *10 m* height.

Sensible and latent heat fluxes are caused by temperature and moisture differences between ocean/ice and atmosphere. Their parameterisations can be written as

$$H = \rho c_p C_H U_z((1 - A)(T - T_s) + A(T - T_{ice})), \quad (3.3)$$

$$E = \rho C_E U_z((1 - A)L_z(q_{10m} - q_s) + AL_{zi}(q_{ai} - q_{si})), \quad (3.4)$$

where c_p is the specific heat of air at constant pressure, C_H stands for the Stanton number, and $T - T_s$ is the temperature difference between the atmosphere and the sea surface; E represents the latent heat flux between the atmosphere/ocean and the

atmosphere/ice (C_E is the Dalton number), q_{10m} - q_s is the difference in specific humidity between the atmosphere and the ocean, and q_{ai} - q_{si} is the difference in specific humidity between the atmosphere and the ice. L_z and L_{zi} are the respective latent heats of evaporation over open water and ice. The transfer coefficients (C_H and C_E) are determined according to Large & Pond (1982). The short-wave radiation (R_{sw}) is approximated by the empirical Zillman equation for clear skies (Zillman 1972). The short-wave radiation flux at the ocean surface, together with the modification due to cloudy skies, is parameterised by:

$$(1 - \alpha)S(o) = (1 - \alpha)R_{sw}(1 - 0.75cl), \tag{3.5}$$

where α is the albedo at the ocean/sea-ice/snow surface (0.03 for the open sea, 0.7 for frozen ice, 0.6 for melting ice, 0.87 for frozen snow and 0.77 for melting snow) and cl is the fractional cloud coverage. The net long-wave radiation is due to atmospheric ($Lw(o)$) and water surface radiation ($Lw(u)$).

$$\begin{aligned} Q_l &= Lw(o) - Lw(u) \\ &= \epsilon\sigma_s[T_s^4 - T^4(a_1 + a_2 e^{1/2})(1 + a_3 cl^2)], \end{aligned} \tag{3.6}$$

where $\epsilon = 0.97$ is the emissivity of surface water, σ_s the Stefan-Boltzmann constant, T_s the sea surface temperature and T the air temperature, e the water vapour pressure, and a_1, a_2, a_3 are constants equal to 0.68, 0.0036 and 0.18, respectively (Hagedorn et al. 2000, Lehmann & Hinrichsen 2000a).

Additionally, river runoff is prescribed from a monthly mean runoff data set (Bergström & Carlsson 1994). Runoff data are specified for 42 separate rivers discharging into the Baltic Sea and the Kattegat. The prognostic variables of the coupled sea-ice-ocean model are sea-ice thickness and compactness, sea-ice drift, the oceanic baroclinic current field, the 3-D temperature, salinity and oxygen distributions, the 2-D surface elevation, and barotropic transport. These prognostic variables were extracted from the model every 6 hours. The model was run for the period 1979-2004 including three field campaigns: February to March 1998, February 2001 and June 2001. Model data were extracted at three different positions in the Baltic Sea in order to allow a minutely detailed comparison with the corresponding observations.

Chapter 4

Interactions of ocean and atmosphere

Atmosphere and Ocean interact with each other through the exchange of energy, momentum and mass. These exchange processes determine the energy and mass budgets of the ocean. Energy is transferred from the atmosphere to the ocean surface mixed layer driving the circulation of the upper ocean and, in turn energy from the ocean is fed back to the atmosphere affecting the atmospheric circulation, the weather and climate. The energy transfer between the ocean and the atmosphere occur both by radiation processes and through turbulent fluxes of sensible and latent heat as well as momentum. In the mass budget minerals, gases and freshwater, which is a combination of evaporation and condensation, precipitation and river runoff, are exchanged.

Here we are only focused on the Baltic See and will describe the water and heat budgets of the Baltic Sea in detail next.

4.1. Water and energy budgets of the Baltic Sea

The Baltic Sea is highly dynamic and strongly influenced by large-scale atmospheric circulation, river runoff and by the restricted water exchange as well as by the complex bathymetry with its narrow straits and channels, strong stratification and heterogeneous sea ice structure. As a consequence, the water balance of the Baltic Sea is mainly controlled by in- and outflow between the Baltic Sea and the Kattegat, river runoff and net precipitation (precipitation minus evaporation). The water balance follows (Omstedt & Rutgersson 2000, Stigebrandt 2001):

$$A_s dz_s/dt = Q_i - Q_o + (P - E)A_s + Q_r + Q_{ice} + Q_{rise} + Q_t + Q_S + Q_g \qquad (4.1)$$

with: A_s : surface Area of the Baltic Sea

z_s : water level of the Baltic Sea

Q_i, Q_o : inflows and outflows through the entrance area

P, E : precipitation and evaporation rates

Q_r : river runoff

Q_{ice} : volume change due to ice advection from the Baltic Sea

Q_{rise} : volume change due to land uplift

Q_T, Q_S : volume changes due to the thermal expansion and salt contraction

Q_g : ground water inflow

Q_{rise} and Q_{ice} are very small terms, but these volume changes can show interannual and decadal variability and have to be considered in long-term water balance studies (Omstedt & Rutgersson 2000).

The heat balance of the Baltic Sea is influenced by the net heat flux between water and atmosphere, the solar radiation into the ocean and through the ice, by the heat flux between water and ice as well as the heat fluxes associated with the in- and outflows through the Baltic Sea entrance area. The heat balance equation reads (Omstedt & Rutgersson 2000):

$$dH/dt = (F_i - F_o - F_{loss})A_s \qquad (4.2)$$

with: H : total heat content of the Baltic Sea

F_i, F_o : heat fluxes associated with in- and outflows

F_{loss} : total heat loss from the water surface

Here the fluxes are positive when going from the water to the atmosphere F_{loss} reads (Omstedt & Rutgersson 2000):

$$F_{loss} = (1 - A_i)(F_n + F_s^o) + A_i(F_w^i + F_s^i) + F_{ice} + F_r \qquad (4.3)$$

where

$$F_n = F_h + F_e + F_l + F_{prec} + F_{snow} \tag{4.4}$$

with: A_i : ice concentration

F_h : sensible heat flux

F_e : latent heat flux

F_l : net long wave radiation

F_{prec} : heat fluxes associated with precipitation in the form of rain

F_{snow} : heat fluxes associated with precipitation in the form of snow

F_s^o : solar radiation to the open water surface

F_w^i : heat flux to the ice

F_s^i : solar radiation through the ice

F_{ice} : heat flux associated with ice advection out from the Baltic Sea

F_r : heat flux associated with river runoff

But, heat is, however, one kind of energy involved in the energy cycle, which also includes various interactions between mean and turbulent kinetic energy, internal wave energy and potential energy. Little is known about how external energy is transformed in the Baltic Sea (Axell 2001).

There is evidence that the interaction of the atmosphere and ocean includes large scale circulation of atmosphere and ocean, as well as smaller scales, mixed layer development and wave generation. Thus, modeling of these interactions always includes surface fluxes, which are difficult to measure directly on small and large scales. Consequently, vertical fluxes of momentum, sensible and latent heat are parameterised in numerical models. Here, the atmospheric boundary layer plays an important role and will nearly comment on next section.

4.2. Atmospheric boundary layer

The atmospheric boundary layer is the lowest part of the atmosphere, which is directly influenced by the surface of the earth and responds to surface forcings with a timescale of about an hour or less (Stull 1988). These forcings include frictional drag, evaporation and transpiration, heat transfer and other contstituents. Also, the boundary layer is dominated by two physical processes. First, the radiative cooling and heating is stronger than in higher levels of the atmosphere. Solar heating leads to turbulent convection and mixing in the boundary layer, whereas cooling at night leads to stabilise the atmospheric boundary layer. The second process is the turbulence. Effectively this means that the wind becomes gusty, which has an important impact on the transport of heat, moisture and aerosols from the surface higher into the atmosphere. Turbulence involves 'random' motions of the air, which are accompanied by fluctuations in temperature and humidity on similar timescales. The vertical wind component is important on the scales at which turbulence acts, i.e. effectively turbulence can stir the air close to the ground.

Further, the configuration of distinct and coherent structures, like convection waves and rolls in the atmosphere, fronts or upper ocean eddies, contribute to the discontinuity and the variability of the exchange processes at the surface. Variation of the atmospheric boundary layer depth is dependent on the surface and variate from tens of meters in strongly statically stable situations, to several kilometers in convective conditions, such as deserts.

4.2.1. Atmospheric boundary layer over open water

The atmospheric boundary layer over water is roughly constant over daily timescales, due to the physical properties of water. These properties mean that the surface energy balance over the sea has some characteristic properties, like the low albedo of water and the emissivity of the water surfaces, which is close to 1. Also, water has a large heat capacity, and conduction/convection to lower levels is very rapid, especially in comparison with land surfaces, i.e. the ocean can absorb large amounts of heat from short-wave solar radiation with relatively little temperature change. The ocean surface is the source for heat and more importantly for water vapour, which enters the air through evaporation.

Consequently, the boundary layer is a crucial component in the hydrological cycle because of the evaporation from the water surface is very efficient. This means, the latent heat flux is larger than the sensible heat flux and the atmospheric boundary layer over water is humid and relatively cool, due to a lot of latent heat in form of water vapour.

An important influence on the boundary layer depth is the air pressure. Generally, the boundary layer is to be thinner in high-pressure conditions than in low-pressure regions (Figure 3). The subsidence and low-level horizontal divergence moves the boundary layer air out of the high towards lower pressure regions. Thin depth are regions with little or no clouds. In low pressure regions the upward motions carry atmospheric boundary layer air away from ground to large altitudes throughout the troposphere, which complicate a definition of a boundary layer top for these situation (Stull, 1988).

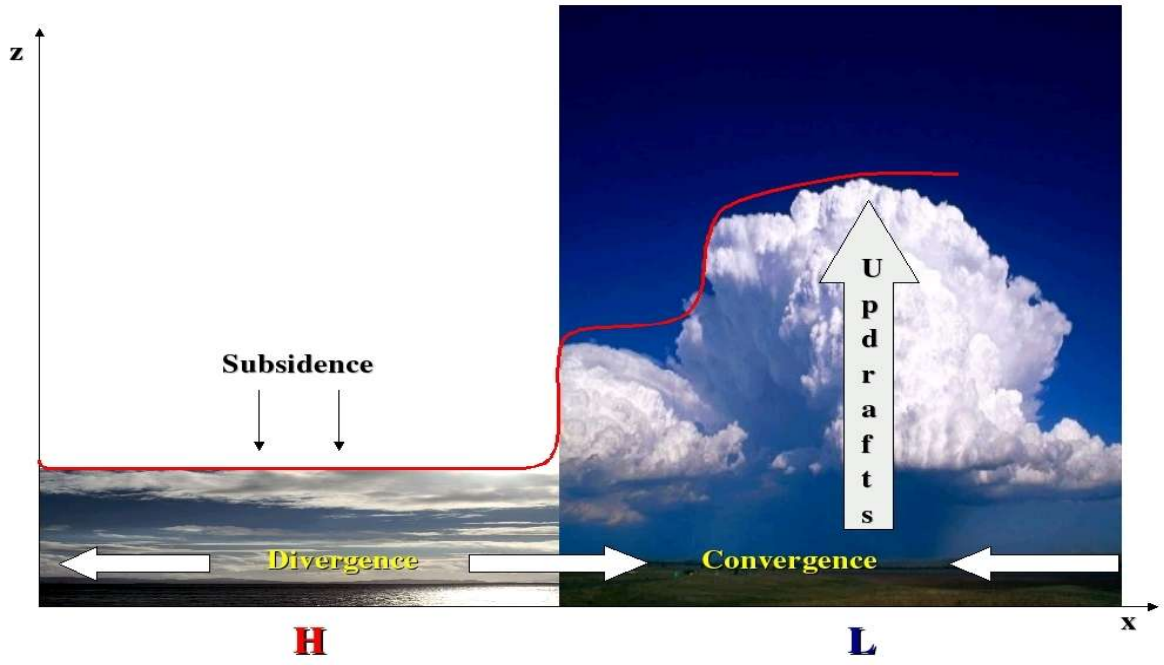

Figure 3. Variation of boundary layer depth between centers of surface high (H) and low (L) pressure. The red line shows the maximum hight in the Troposphere reached by modified air during a one-hour period.

4.2.2. Heat and radiation budget

The ocean surface is a material interface that is a barrier for exchange of heat, moisture, momentum and trace constituents. Atmosphere and ocean are in turbulent motion, but near the interface turbulence is suppressed and transport is generally regulated by molecular processes. The fundamental processes that connect the atmosphere and the ocean are the energy input to the ocean by the wind, the net freshwater flux and the net surface heat flux.

The heating of the lower part of the atmosphere depends on the heating of the surface and the transport of the heat from the surface into the air. The surface energy balance is determined by the different fluxes (flows) of heat energy at the surface, which is seen in equations (4.2)-(4.4). Latent and sensible heat fluxes are both important in the heat budgets of the atmosphere and ocean, they are the sources of energy, especially for the troposphere. Latent heat flux is released in clouds, at higher levels and affects indirectly both cloud and rain formation and warms the middle of the troposphere. In contrast, sensible heat warms the boundary layer directly, that means the sensible heat flux over a certain surface type affects the air temperature, and due to the advection in the atmosphere this effect is felt in the sensible heat flux over the neighbouring surface types (Vihma 2005). Further, sensible heat flux is one of the parameters controlling the height of the mixed layer (Rutgersson et al. 2001).

The ocean heat budget behaves differently than the land budget, because turbulence in the water can efficiently transport heat away from the surface and distribute it deeper in the water. Also, the heat capacity of water is about 4000 times larger than that of air, meaning that a lot of heat can be absorbed into water with little temperature change. Thus the diurnal cycle of radiation is almost completely balanced by a corresponding diurnal variation of energy transport into the sea. In addition, the nearly constant sea surface temperature with time results in a nearly constant heat and moisture flux, and associated slow temporal changes in air temperature and humidity. (Stull 1988)

The incoming solar radiation at the top of the atmosphere is determined by orbital variations in the distance between the earth and the sun as well as by the altitude of the sun. Some of the incoming radiation in the atmosphere is reflected and absorbed through clouds and aerosols. Clouds affect directly the net short-wave and net long-wave fluxes at the surface. Changes in cloud properties affect the surface energy balance. These changes in surface energy fluxes modify, in turn the temperature, humidity, density, pressure and wind in the lower atmosphere, thereby closing the feedback loop.

4.3. Sea-ice

In the climate system, sea ice is an important component and highly sensitive indicator of climate variability and change (Vihma 2005). A sea ice cover is seldom uniform, it consists of ice floes of varying thickness, leads and polynyas. The surface conditions are affected by interacting dynamical and thermodynamical processes. The surface may change rapidly due to ice dynamics, like advection and deformation or slower changes, such as thermodynamics (ice formation, growth and melt) and precipitation. To understand the reflection, absorption and transmission of short-wave radiation by sea ice, it is important to know something about ice thermodynamics and ice climatology.

4.3.1. Properties and structure of sea ice

Sea ice is a translucent material with a sophisticated structure and complex optical properties (Figure 4). Absorption and scattering are a combination of radiation transition. Scattering determine differences in the range of sea ice, whereas absorption is the cause of spectral variations. Changes in the state and microstructure of the ice, specifically those of brine, gas and salt inclusions, are directly related in properties, such as the albedo, reflection, transmittance and extinction.

Sea ice is often covered by snow, and if the snow cover is new and dry, the albedo can be up to 0.9, while the albedo of melting bare ice is only of the order of 0.4 or less, if the ice has become very thin, in contrast, the albedo of the open sea is typically below 0.1 (Vihma & Haapala 2005). Changes on the snow/ice surface are accordingly associated with a strong feedback mechanism. If ice is present, the rate of exchange of heat and gases (e.g., CO_2) between the atmosphere and the ocean is greatly reduced. In winter the air-water temperature difference through the ice and snow can be up to 30 K.

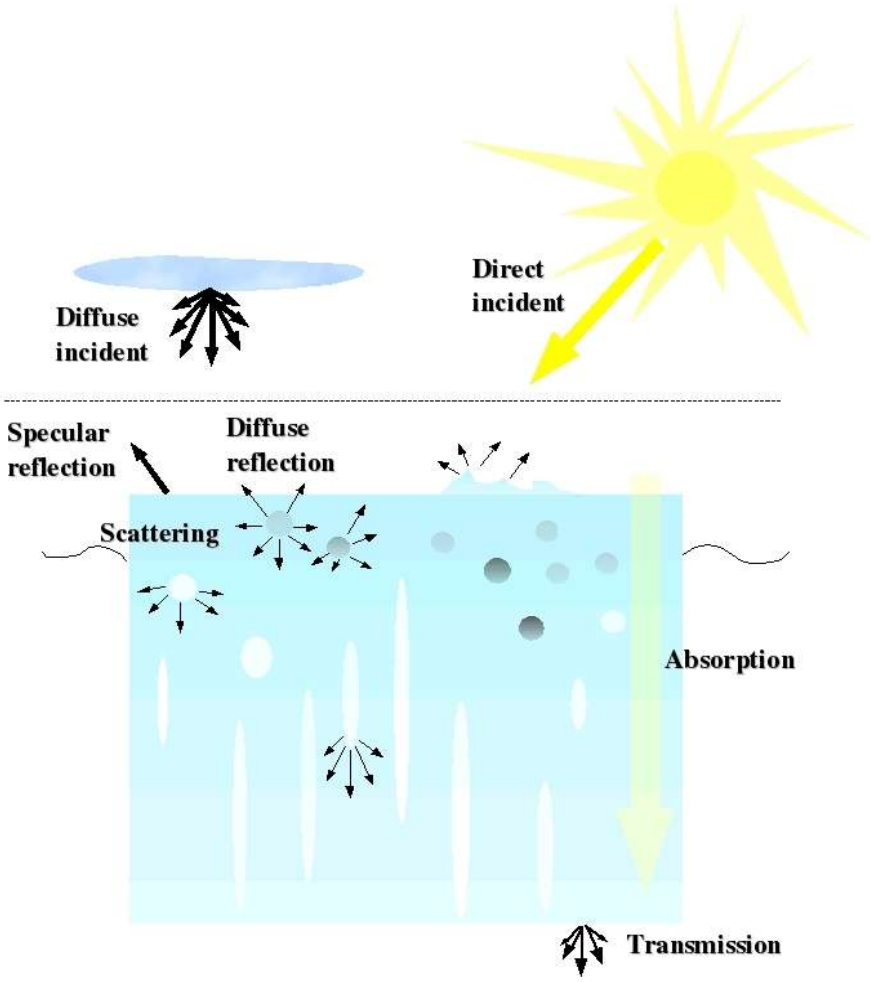

Figure 4. Schematic depiction of sea ice radiative transfer processes

Sea ice cover is seldom uniform, but broken by cracks, leads and polynyas, which act as pathways for heat and moisture from the ocean to the atmosphere. Also, the ice pack stores and advects fresh water, heat, atmospheric settling and sediments, and may release them far away from their original source (Vihma & Haapala 2005). In addition, the extend and limited thickness of sea ice cover are particularly sensitive to changes in temperature and ocean heat flux.

The Baltic Sea ice is a special ice type and cannot be described by one ice type only (Brümmer et al. 2002), because it is formed out of brackish water (salinity less than 24.7 PSU). Figure 5 represents different ice characteristics in the northern Baltic Sea in March 2006. Ice formation starts in the northern part of Bothnian Bay. Fast ice forms and remains along the coast, where it is attatched to the shore or to the archipelago. It develops relatively rapidly during the freezing period and may be formed in situ from sea water or by freezing of drift ice to the shore and remains

fairly stationary for most of the ice season.

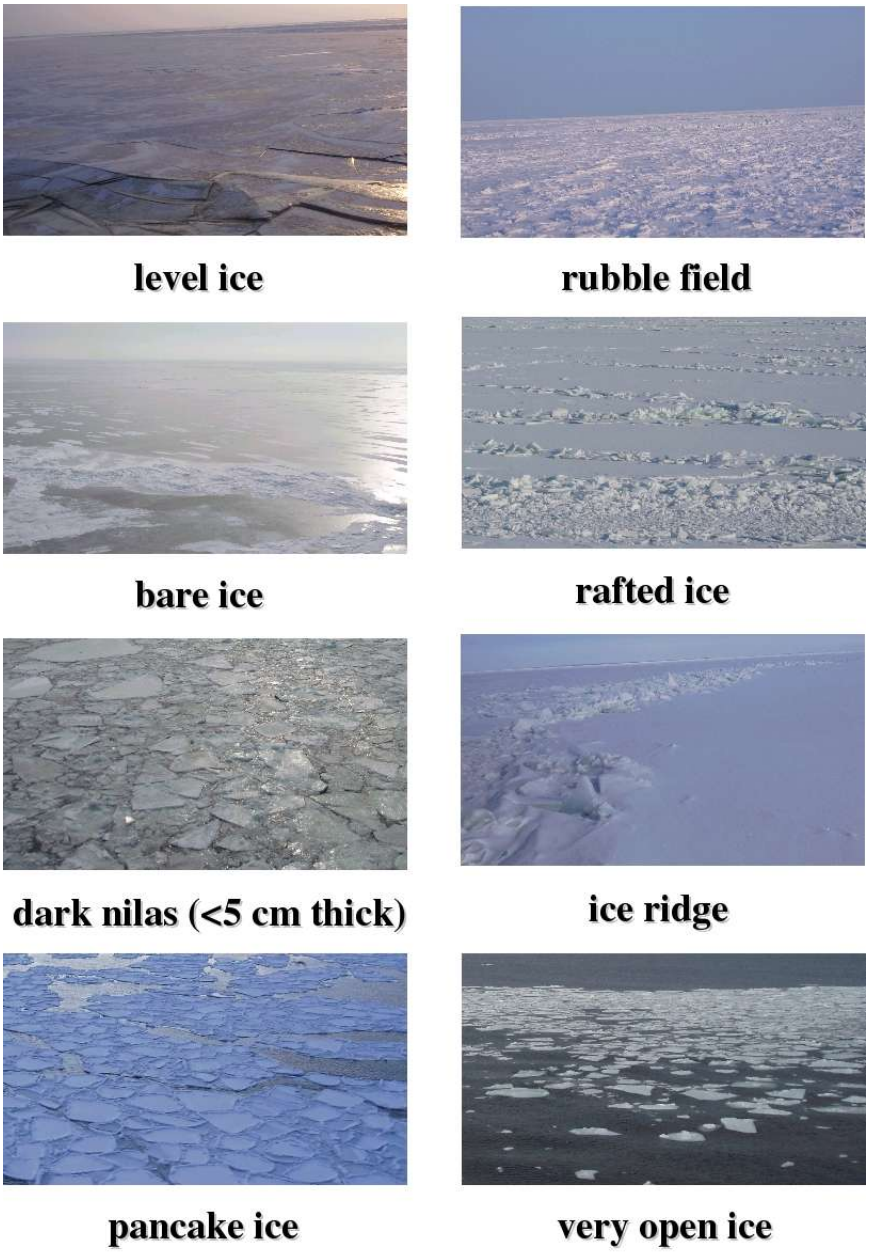

Figure 5. Different ice characteristics in the northern Baltic Sea in March 2006.

Level ice may form on the open sea and has not been affected by deformation, but more often wind and waves prevent the newly formed floating ice and broken pieces striking against one another, and the result is pancake ice with raised rims (Figure 5). If the weather is clear, without snow or wind, bare ice may be formed (Figure 5). In contrast, rafted ice is formed from level ice floes compressed, overriding another and rafted by the wind. Often a line or wall of broken ice forced up by pressure, may be

fresh or weathered (ice ridge in Figure 5). The thickness of ridges is ranging from 1 m – 10 m and more. The height of ridges created from thick ice depends mostly on the pressure force whereas the height of thin ice ridges depends more on the ice thickness of the ice (Kankaanpää 1988). The knowledge of ridging characteristics is an important factor in the understanding and modelling of the Baltic Sea, due to the large mass of the ridged ice, accounting for 10-50% of the total ice mass (Leppäranta & Hakala 1992, Omstedt 2001). Further, areas of extremely deformated sea ice of unusual thickness formed during the winter by the motion of drift ice against, or around a protruding rock, islet or other obstruction, these areas are named rubble fields (Figure 5). But, during melting or strong wind conditions very open or close ice fields may be drifted away from the coast or break from the fast ice edge.

The salinity of the brackish water ice is typically >0.5 PSU in the Bothnian Bay and increases to the South (Palosuo 1961). When sea ice forms, the salt is excluded and cold and dense brine sink down in brine drainage channels which generally form in the direction growth. In general, the salinity in the solid ice decreases through the season, implying that the brine passes out of the ice. At the same time, the salinity of the brine increases as more ice is separated, but the total salinity decreases as the ice grows older (Lundin & Håkansson 2000).

The structure, properties, thermodynamics and dynamics of sea ice are closely interrelated, whereas sea ice and snow thermodynamics are controlled by the exchange of heat at the ice-ocean and air-snow interfaces (or, in the case of bare ice, at the air-ice interface), penetration of solar radiation below the snow/ice surface, and by the conduction of heat inside the snow and ice (Vihma & Haapala 2005).

4.3.2. Atmosphere-ice interaction

The atmospheric boundary layer plays an important role as a buffer between the sea ice and the bulk of the atmosphere (Vihma 2005). During cold air outbreaks the atmospheric boundary layer is strongly affected by heat fluxes from leads (Vihma & Bümmer, 2002). During such fracture or passage-ways through sea ice, the upwind snow/ice surface is typically close to a thermal equilibrium with the atmospheric boundary layer. If the thermal equilibrium broken down, for example during cold air advection over warm water an energy compensation takes place which is visible as sea smoke (Figure 6).

Ice and snow fundamentally alter the interaction processes (Smith et al. 1996). Sea ice and snow cover inhibits the radiation of heat from the relatively warm ocean to

the cold polar atmosphere. Thick sea ice (>1 meter) is a good isolator, it can prevent more than 95% of the heat loss from the sea.

Figure 6. Sea smoke in the Bothnian Bay in March 2006 (Picture. Anja Neutzling)

The spatial variability of the fluxes is caused by the ice/water inhomogenity (Brümmer et al. 2002). Thin ice, leads and polynas have important consequences on regional heat budgets. Even open water within the ice pack is often a location of very high heat flow from ocean to atmosphere. This energy is released as sensible heat flux from the warm ocean and as latent heat as surface water freezes. So that, the fluxes depend on the large scale weather conditions and on the state of the surface. The spatial variability of heat fluxes in the ice edge zone is small during warm-air advection ($T > 0°C$) and melting conditions, there are no heat flux differences between ice and water, because both surfaces have about the same temperature. During cold-air advection ($T < 0°C$), the spatial variability of the heat fluxes is large, because ice and water have different surface temperatures, heat fluxes are different over ice and water and the difference increases with decreasing air temperature (Brümmer et al. 2002).

Another important fact is the surface roughness of sea ice. It is determined by its thermal and dynamic history. Flat, level ice has about the same aerodynamic roughness and drag coefficient as open water at moderate wind speeds (Smith et al. 1996). Ice rubble fields, like in Figure 5, have air drag coefficients up to 4 times

greater than flat ice (Anderson 1987). Roughness elements are even larger on the lower than on the upper surface of sea ice. Divergent forces open up leads between the floes, where even a few percent of open water can provide the pathway for the majority of sensible, latent and radiant heat fluxes through the surface (Smith et al. 1990).

In general, in the presence of sea ice the energy budget is balanced by freezing or melting of sea ice and is defined as:

$$Q_a + Q_o + \rho_i L_i \partial h/\partial t = 0 \qquad (4.5)$$

with: Q_a : atmospheric heat flux

Q_o : heat flux from the deep ocean

ρ_i : density of sea ice

L_i : specific heat of fusion for sea ice

$\partial h/\partial t$: growth rate of sea ice

The most important unknowns in the surface energy balance involve the disposition of the energy inputs in the ocean with sea ice during the melting season, especially the effects on the upper ocean and surface albedo. Further, the understanding of energy utilization within the ice-ocean system is important and will discussed next.

4.3.3. Ice-ocean interaction

The freezing temperature of seawater depends on salinity. The growth of sea ice further influences the ocean by rejecting salt to the underlying water, leading to increased water density directly below the ice. The fluxes between the ice and ocean mixed layer are principally dominated by the very thin viscous boundary layer next to the ice. Across this interface the gradients of temperature and salinity are greatest. By regulating the temperature at the interface to be always near freezing, sea ice provides a strong restriction on heat flux in the upper part of the oceanic boundary layer. The main elements of enthalpy conservation at the ice-ocean boundary are

conduction of heat through the ice, balanced by latent heat changes through freezing or melting at the interface, and upward heat flux from the ocean. The oceanic heat flux at the lower ice surface depends primarily on the difference in temperature between the undisturbed fluid at the far extent of the boundary layer, characterized by friction speed at the interface. Sea ice rejects most of the salt as it freezes, thus melting can have a significant effect on heat transfer, first by elevating the freezing temperature at the interface relative to the freezing temperature in the mixed layer, because the salinity is less than there in the mixed layer proper and second by stabilizing the turbulent boundary layer so that the efficiency of turbulent exchange is diminished. Further, heat and salt flux respond to actual levels of turbulent stress in the boundary layer, as opposed to the speed of ice drift relative to the underlying ocean (McPhee 1992).

Chapter 5

Parameterisation of turbulent processes

Parameterisation means the development of simplified mathematical representations, using experimental results and fundamental concepts to define unknown physical processes. Parameterisation must:

(i) have the same dimension as the unknown

(ii) have the same tensor properties

(iii) have the same symmetries

(iv) be invariant under an arbitrary transformation of coordinate systems

(v) be invariant under a Galilean transformation

(vi) satisfy the same budget equations and constants (Stull 1988).

For most purposes, direct measurements of turbulent surface fluxes of momentum, sensible and latent heat between the atmosphere and the ocean surface are very difficult to obtain. Parameterisations can used instead to estimate fluxes from more readily available data. Surface-layer scaling parameters for wind, temperature and humidity are most easily measured in the atmospheric surface layer, whose dynamical properties are well described by Monin-Obukhov similarity theory. Because of the direct influences of the bottom boundary, the important parameters are the height z, the mean air density ρ and the turbulent transports through the layer, which are defined by the Reynolds fluxes:

$$\tau = -\rho\langle uw\rangle \qquad (5.1)$$

$$H = \rho C_p \langle wt \rangle \tag{5.2}$$

$$E = L_E \langle wq \rangle \tag{5.3}$$

with: τ : wind (surface) stress

H : sensible heat flux

E : latent heat flux

ρ : air density

$\langle uw \rangle$: time average of velocity momentum flux

C_p : specific heat at constant pressure of dry air

$\langle wt \rangle$: time average of temperature flux

L_E : latent heat of evaporation

$\langle wq \rangle$: time average of moisture flux

Other relevant quantities are the sea surface temperature T_s, the absolute humidity at the surface q_s and the potential temperature θ.

According to the Monin-Obukhov constant flux layer, the dimensionless profile gradients for velocity, temperature and water vapour in the surface boundary layer can be written as follows:

$$u^* = (\tau/\rho)^{1/2} = |\langle uw \rangle|^{1/2} \tag{5.4}$$

$$t^* = -H/\rho C_p k u^* = -\langle wt \rangle (ku^*)^{-1} \tag{5.5}$$

$$q^* = -E/\rho k u^* = -\langle wq \rangle (ku^*)^{-1} \tag{5.6}$$

with: u^* : friction velocity

t^* : temperature scale

q^* : humidity scale

k : Kármán constant (= 0.40)

The quantities normalized with these parameters are unique functions of the dimensionless height z/L, where L is the Monin-Obukhov length:

$$L = -u^{*3}T_0(kg\langle wT_v\rangle)^{-1} \tag{5.7}$$

with: T_0 : local average of the virtual temperature

g : gravitational acceleration

T_v : virtual temperature in degrees Kelvin

$\langle wT_v\rangle$: vertical flux of virtual temperature

In this form the theory is only valid for dry air. For moist air, the flux of virtual temperature replaces the 'normally' temperature flux. The mean gradients are universal functions of the stability parameter z/L and may be expressed as:

$$(kz/u^*)\,(\partial\langle U\rangle/\partial z) = \varphi_m(z/L) \tag{5.8}$$

$$(z/t^*)\,(\partial\langle\theta\rangle/\partial z) = \varphi_t(z/L) \tag{5.9}$$

$$(z/q^*)\,(\partial\langle Q\rangle/\partial z) = \varphi_q(z/L) \tag{5.10}$$

with: $\partial\langle U\rangle/\partial z$: mean wind gradient

$\partial\langle\theta\rangle/\partial z$: mean potential temperature gradient

$\partial\langle Q\rangle/\partial z$: mean humidity gradient

φ_m, φ_t, φ_q : universal functions

The so-called universal functions characterize the effects of the atmospheric surface layer stratification, in terms of the Obukhov length L, on the profile gradients and build a basis of surface fluxes parameterisation.

5.1. Bulk method

Empirical coefficients are used to estimate fluxes from gradients using profile data from only one level in the air and one in the water, whereas the bulk method can be used to estimate fluxes from historical sets of marine weather observations of bulk variables, like wind, humidity, air and water temperatures. The integration of the profile gradients (5.8, 5.9, 5.10) with respect to the height z yields the bulk aerodynamic formulas for the turbulent fluxes of momentum (τ), sensible heat (H) and evaporation (E). They are generally formulated as:

$$\tau = \rho C_D U_z^2 \tag{5.11}$$

$$H = \rho c_p C_H U_z(\theta_s - \theta_z) \tag{5.12}$$

$$E = \rho C_E U_z(q_s - q_z) \tag{5.13}$$

with: U_z : wind speed at a height of z

C_D : drag coefficient

C_H : Stanton number

C_E : Dalton number

$\theta_s - \theta_z$: difference in potential temperature between the atmosphere and the surface

$q_s - q_z$: difference in specific humidity between the atmosphere and the surface

The nondimensional bulk transfer coefficients (drag coefficient C_D, Stanton number C_H, Dalton number C_E) are functions of height and stability and they can be expressed as:

$$C_D = [k/(\ln z/z_0 - \Psi_m)]^2 \tag{5.14}$$

$$C_H = [k/(\ln z/z_0 - \Psi_m)]\,[k/(\ln z/z_T - \Psi_t] \tag{5.15}$$

$$C_E = [k/(\ln z/z_0 - \Psi_m)]\,[k/(\ln z/z_{0q} - \Psi\,] \tag{5.16}$$

with: z_0 : surface roughness length for wind speed

z_T : surface roughness length for temperature

z_{0q} : surface roughness length for water vapour

Ψ_m, Ψ_t, Ψ : integrated universal functions

For air-sea interaction parameterisations by bulk formulas, the local aerodynamic roughness lengths (z_0, z_T) or the local bulk transfer coefficients (C_D, C_H) must be known. The bulk calculation leads to an iterative solution, except in a rough first-order estimation not taking the stability explicitly into account. Additionally, it is usually assumed by theoretical arguments, that the bulk coefficient $C_H = C_E$. In other words the roughness for heat follows close to that of moisture. However, for most of the surfaces, the thermal roughness length is smaller than that for momentum, because heat and momentum transfer are calculated by different processes, in order that $C_D \neq C_H$.

The roughness length z_0 describes the surface as „seen“ by the turbulence and it may be a complicated function of sea surface parameters (Burling & Stewart 1967). In practice the transfer coefficients must be determined from direct flux measurements and the mean or bulk quantities. Wave observations are seldom available, so it is customary to relate z_0 or the neutral drag coefficient C_{DN} to the mean wind speed.

At a heigth z, the mean wind Uz, is found by integrating (5.8) (Paulsen 1970):

$$Uz = [u*/k][ln(z/z_0) - \Psi_m(z/L)],$$

where

$$\Psi_m(z/L) = \begin{cases} 5z/L, & stable\ (z/L > 0) \\ 2\ ln[(1 + X)/2] + ln[(1+X^2)/2] & \\ 2\ tan^{-1}X + \pi/2, & unstable\ (z/L < 0) \end{cases}$$

with

$$X = (1 - 16z/L)^{1/4} \qquad (5.17)$$

To eliminate its variation with height, the drag coefficient is commonly evaluated in the equivalent neutral case at 10 m, using the wind speed at 10 m, obtained from (5.17) (Large & Pond 1981). So that, empirical formulations of neutral transfer

coefficients, which can be parameterised in different ways, allow the turbulent heat fluxes to be estimated from U_z, θ_z or T_z, Q_z and *Ts* using the Reynolds fluxes (5.1, 5.2, 5.3) and the bulk aerodynamic formulas (5.11, 5.12, 5.13) (Large & Pond 1981).

Generally, the bulk method is the only practicable way to calculate surface fluxes in numerical models, but the values of the transfer coefficients are the most important factors, because they are responsible for the representation of the flux processes. Some not completely understood processes in the ocean surface layer, such as the influence of waves for limited fetch, are the reason for a large scatter in estimates of the heat transfer coefficients. Some investigations have been performed in coastal or shallow areas, but the heat transfer coefficients are not expected to be as sensitive to limitations in water depth (Rutgersson et al. 2001). Most of the studies show relatively small variations with wind speed, but a slight effect of high winds cannot be ruled out (DeCosmo et al. 1996, Makin 1998). Further, for low winds, smooth surface effects and gustiness also appear to increase the transfer coefficients (Beljaars 1994). In some studies (Large & Pond 1982, Smith 1988, 1989, Rutgersson et al. 2001) the validity of the transfer coefficients were tested on different ways. Rutgersson et al. found that the neutral stanton number is, $C_{HN\text{-}unstab} = (1.0 \pm 0.3) \times 10^{-3}$ for the unstable and $C_{HN\text{-}stab} = (0.77 \pm 0.5) \times 10^{-3}$ in stable stratification, which is close to that found by Large and Pond (1982). As a mean for all data, they found $C_{HN} = (1.0 \pm 0.3) \times 10^{-3}$ and for the Dalton Number $C_{EN} = (1.2 \pm 0.2) \times 10^{-3}$. The drag coefficient is an adequate description of most results throughout the wind speed range 4-12 m/s at 10 m height. Large and Pond (1982) found a reasonable average, $C_{DN} = 1.2 \times 10^{-3}$ for wind below about 11 m/s. Schröder et al. calculated the transfer coefficients at 10 m height over sea ice. They found the following mean values (± standard deviations), $C_{DN} = (1.9 \pm 0.8) \times 10^{-3}$, $C_{HN} = (0.9 \pm 0.3) \times 10^{-3}$ and $C_{EN} = (1.0 \pm 0.2) \times 10^{-3}$. These studies and values show the difficulties and uncertainties in the accurate determination of the transfer coefficients and depend on the accuracy of the measured data. Also, it is known that the determination of C_{HN} is particularly sensitive to surface temperature measurement errors [e.g., Calanca 2001] (Schröder et al. 2003).

Surface fluxes in the Baltic Sea-Ice-Ocean Model (BSIOM) have been calculated with the bulk method, using transfer coefficients after Large and Pond (1981) (see Chapter 3, equations 3.2-3.4), to compare measured and calculated fluxes.

The atmosphere-ocean or land-atmosphere fluxes play an important role in coupled models. In an ice-ocean model, surface fluxes between atmosphere and ocean drive the ocean model and in the atmospheric model sea surface temperature drive the model. In order to validate such coupled model systems, comprehensive data sets are

required. However, in this work model data have been extracted at different positions in the Baltic Sea in order to allow a carefully detailed comparison with corresponding observations.

Chapter 6

Experiments over the Baltic Sea

During the period 1998-2001 over the open and ice-covered water of the Baltic Sea eight experiments were performed with the overall objective of collecting a comprehensive data set suitable for validating the BALTIMOS coupled model system (**BALT**ic Sea **I**ntegrated **MO**del **S**ystem, Brümmer et al. 2003) for the Baltic Sea region. BALTIMOS was developed within the framework of BALTEX/DEKLIM (German Climate Research Programme 2001-06) by linking existing model components for the atmosphere (REMO model), for the ocean including sea-ice (BSIOM model), for the hydrology (LARSIM model) as well as for lakes.

Times and names of the eight experiments are:

BASIS 1998	17 February - 6 March 1998
Alkor 4/2000	5 – 10 April 2000
Alkor 6/2000	14 – 20 June 2000
Alkor 10/2000	25 – 31 October 2000
BASIS 2001	12 – 23 February 2001
Alkor 4/2001	2 – 11 April 2001
Alkor 6/2001	12 – 20 June 2001
Alkor 10/2001	29 October – 7 November 2001

The Winter experiments were conducted within BASIS (Baltic Air Sea Ice Study, Brümmer et al. 2003), the other six experiments over open water have been conducted on RV Alkor.

6.1. BASIS (Baltic Air Sea Ice Study) 1998

During the first BASIS field experiment, lasting from 16 February to 6 March 1998, turbulent heat, moisture and momentum fluxes as well as radiation fluxes were measured over ice and water in the northern Baltic Sea (Brümmer et al. 2002). The locations of the ice measurement stations Kokkola and RV Aranda, situated about 80 km apart, are shown in Figure 7. The Kokkola ice station was placed on land-fast ice about 4 km south of the island of Vallgrund and at a distance of about 30 km from the ice edge. The time interval of the measurements at the two stations was 10 minutes, whereas calculated values are given at 6-hour intervals.

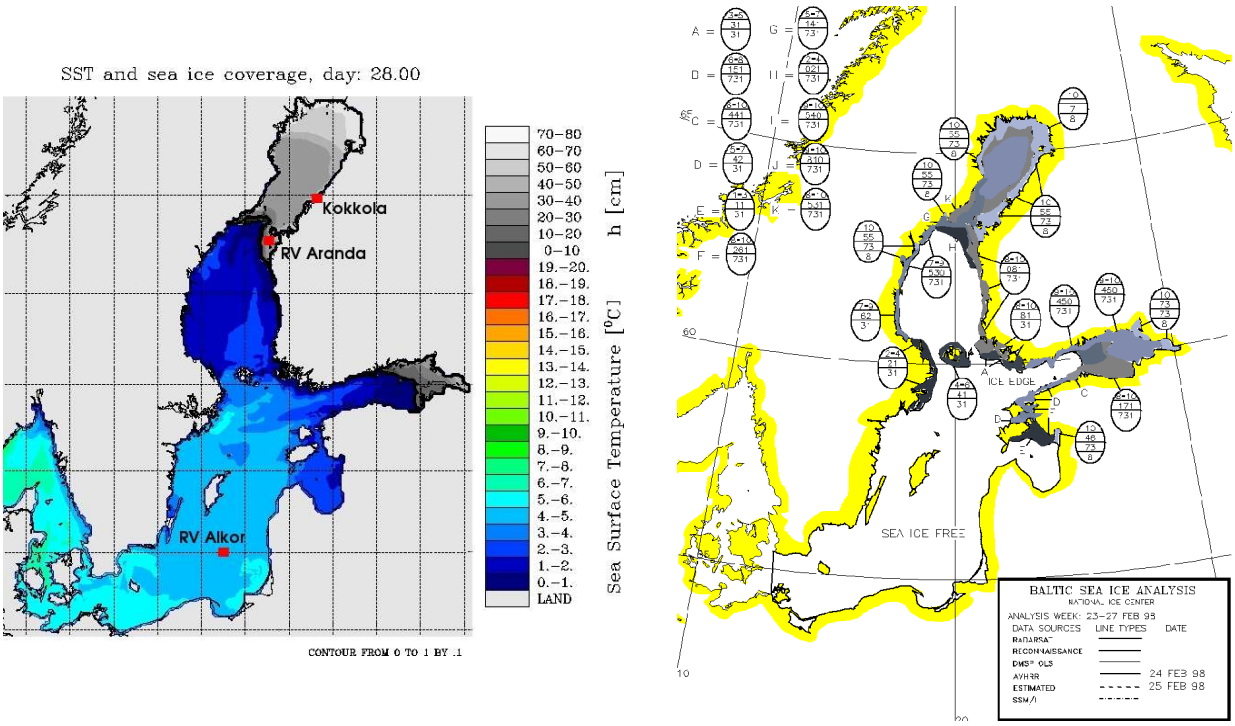

Figure 7. Simulated SST and sea-ice extent (grey colours – sea-ice thickness; contour lines – sea-ice concentration) on 28 February 1998 with positions of the ice stations Kokkola and RV Aranda, as well as RV Alkor (right). Baltic Sea-ice analysis (sea-ice concentration) by the US National Ice Center for 24 February 1998 (left).

The 1997-98 sea-ice season was generally normal, except in the northern Bay of Bothnia and the eastern Gulf of Finland, where ice began to form about a week earlier than usual. The ice cover reached its largest extent – 129 000 km² – on 11 March (Kalliosaari 2002a). During the experiment, sea ice conditions with respect to sea ice extent varied only slightly. The sea-ice extent on 28 February 1998 (Figure 7 left) can therefore be taken as representative of the sea-ice situation during this

period. The simulated sea-ice extent agrees well with field observations (see Figure 1 in Brümmer et al. 2002) and the satellite analysis of sea-ice (Figure 7 right), but in the Gulf of Finland and the Gulf of Riga the ice extent was somewhat underestimated.

6.1.1. Evolution of meteorological quantities

During BASIS 1998, meteorological conditions in the experimental area were characterized by a rapid sequence of high and low pressure systems and passing atmospheric fronts. Figure 8 shows the time series of the basic meteorological quantities pressure *p*, temperature *T*, water vapour mixing ratio *m*, wind speed *U* and wind direction *Wind Dir* at Kokkola and RV Aranda. Steady weather conditions lasted no longer than one day.

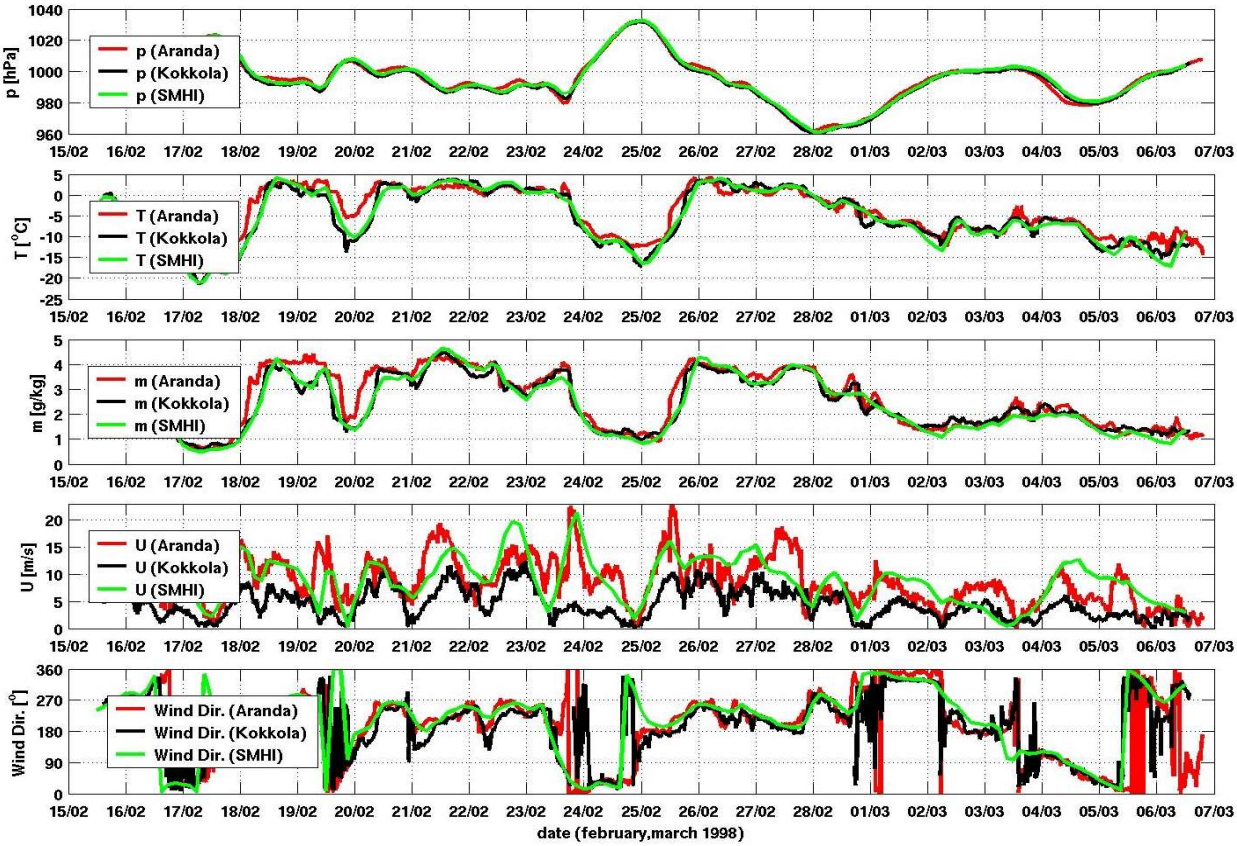

Figure 8. Time series of pressure *p*, temperature *T*, water vapour mixing ratio *m*, wind speed *U* and wind direction *Wind Dir* at Kokkola and RV Aranda in comparison with observed atmospheric data (SMHI meteorological data base) at Kokkola.

In the rear of lows, passing close to or directly over the experimental area, air temperatures decreased rapidly to below 0°C (17, 19, 24 February), as well as water vapour mixing ratio drops under 1 g/kg. These three cold episodes lasted only one or two days and were brought to an end by approaching warm fronts, respectively which can be associate with rising of U up to 19 m/s and changing of wind direction from north to west. Extracted atmospheric (SMHI forcing) data at Kokkola compare well with corresponding measurements. However, wind velocities agree better with the RV Aranda measurements owing to the different measurement heights (Kokkola 2 m, RV Aranda 19 m).

6.1.2. Radiation fluxes

The temporal evolution of surface fluxes measured at Kokkola and on RV Aranda is presented in Figure 9. Although these two stations were only 80 km apart from each other, there are obvious differences, which might have been due to differences in cloud cover. Differences in cloud cover also have caused the discrepancies between the calculated (BSIOM) and measured values. The albedo of the ice/snow surface varied between warm and cold episodes with some time delay. Periods of high albedo during freezing periods (white ice surface) and low albedo during melting periods when the ice surface is widely gray instead of white can be discriminated. Tendencies of modelled albedo compare well with observations.

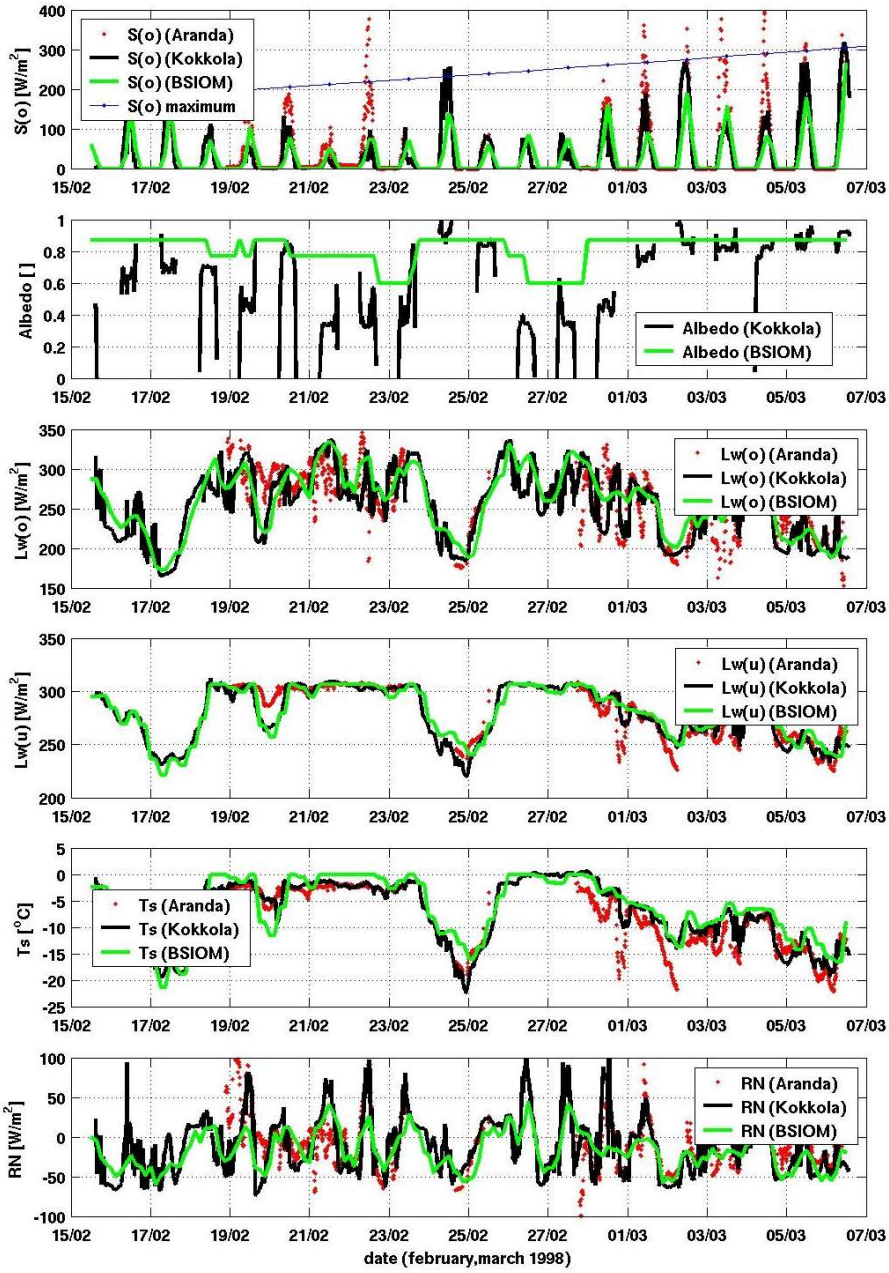

Figure 9. Time series of short-wave radiation *S(o)* (the blue line represents the daily clear sky *S(o)* maximum at Kokkola), albedo, downwelling long-wave radiation *Lw(o)*, upwelling long-wave radiation *Lw(u)*, surface temperature T_s and net radiation *RN* at Kokkola and RV Aranda in comparison with model data at Kokkola.

The downwelling long-wave radiation flux *Lw(o)* is closely related to the varying cloud conditions. During warm periods with low-level clouds (e.g., about 325 Wm^{-2} on 21 February) and during cold air periods with clear skies (e.g., about 175 Wm^{-2} on 25 February) *Lw(o)* exhibits extreme values. Calculated (BSIOM) long-wave radiation fluxes agree well with local observations. Compared to *Lw(o)*, the

variability of the upwelling long-wave radiation flux *Lw(u)* is smaller, although extreme values also occur at the same time in relation to the changing weather conditions. The surface temperature T_s shows approximately the same structure as the air temperature (Figure 8). Calculated sea-ice surface temperatures compare well with observations.

The net radiation flux, $RN = S(o) - S(u) + Lw(o) - Lw(u)$, varies with the daily cycle and clouds. Day values were positive (e.g., 22 February at Kokkola), whereas night values were predominately negative (e.g., 25, 27 February at Kokkola). The comparison of net radiation fluxes reveals the largest deviations, because small differences in short-wave radiation and downwelling long-wave radiation lead to larger discrepancies, although the overall structure is well covered.

6.1.3. Turbulent Fluxes

Turbulent fluxes of heat and momentum are presented in Figure 10. Sensible heat fluxes reflect the advection of warm and cold air masses due to moving lows and passing fronts. The sensible heat flux *H* varies approximately between -110 Wm^{-2} and 100 Wm^{-2}. Positive values were the result of melting weather conditions (e.g. 20/21, 22 and 25/26 February) with high wind speeds, and negative values occurred when the air temperature dropped rapidly below 0 °C in the rear of passing lows.

The latent heat flux *E* was not measured, so only the calculated latent heat fluxes are displayed. The latent heat flux *E* at Kokkola was calculated by the same bulk formula as in BSIOM (equation 3.4) using the water vapour mixing ratio *m* and the air-surface temperature difference $T\text{-}T_s$. At RV Aranda, however, *E* was calculated by the bulk aerodynamic method presented by Launiainen & Vihma (1990). Latent heat fluxes varied mostly between -80 Wm^{-2} and 130 Wm^{-2}. Negative values occurred when the air temperatures were above freezing (e.g. 19, 21 and 26 February), causing snow to melt and eventually melting ponds on the sea-ice leaving patches of melt water on the sea-ice.

The momentum flux reflects the wind speed variations caused by synoptic variability. Extreme values occurred on 24 February during the passage of a cold front. Surprisingly, the measured values are much higher compared with calculated values, although the wind speed on 24 February were in relatively close agreement (wind measurements at Kokkola did not show a maximum at all - Figure 8).

The air-surface temperature difference $T\text{-}T_s$ reflects the direction of the sensible heat

flux. Although the overall structure of measured and calculated differences agree quite well, there are larger differences up to 10°C. These differences are mainly due to deviations of calculated sea ice surface temperatures from the observations.

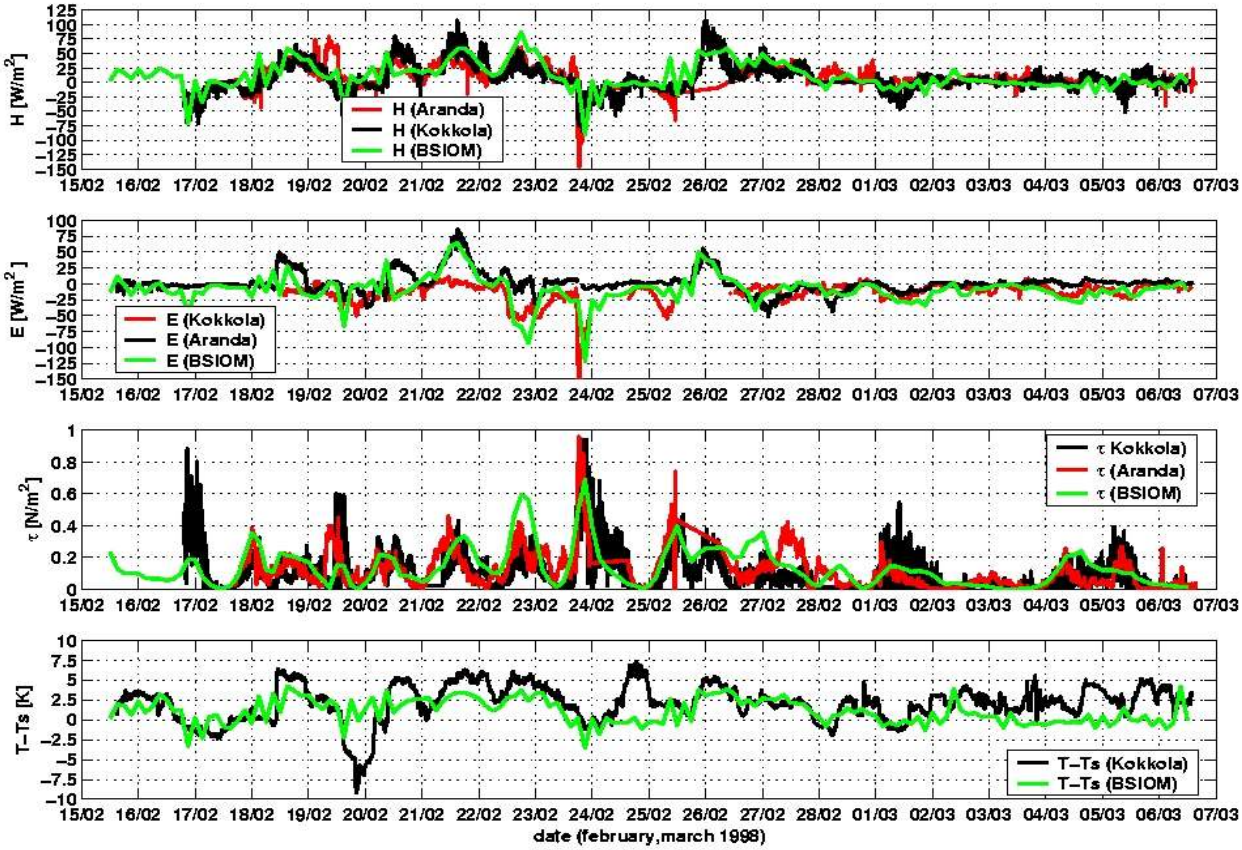

Figure 10. Time series of sensible heat flux *H*, latent heat flux *E*, momentum flux τ and air-surface temperature difference T-T_s at Kokkola and RV Aranda in comparison with model data at Kokkola.

6.2. BASIS (Baltic Air Sea Ice Study) 2001

The BASIS field experiment 2001 lasted from 12 February to 23 February 2001. The ice season 2000-01 was mild and shorter than average. The maximum ice extent reached 128 000 km² (Kalliosaari, 2002b). Figure 11 shows a comparison of the ice situation on 19 February 2001 between the simulated SST (Figure 11 left) and the Baltic Sea-ice analysis of the US National Ice Center (Figure 11 right). Simulated and observed ice extent agree reasonably well, but in the simulation no ice is present in the Gulf of Riga and the ice extent in the Gulf of Finland is somewhat underestimated (Figure 11 left).

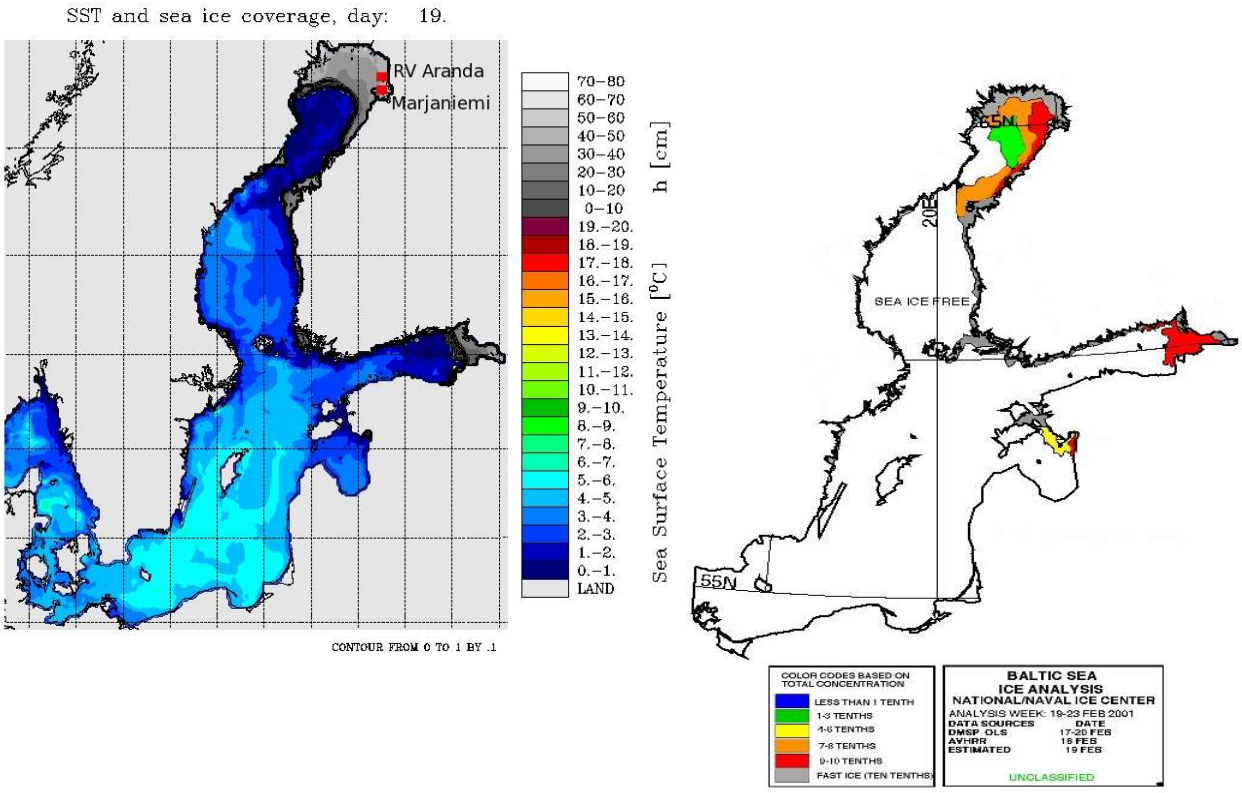

Figure 11. Simulated SST and sea-ice extent (grey colors – sea-ice thickness; contour lines – sea-ice concentration) on 19 February 2001 with positions of the ice stations Marjaniemi and RV Aranda (left). Baltic Sea-ice analysis (sea-ice concentration) of the US National Ice Center for 19 February 2001 (right).

The Marjaniemi Station was located on the west side of the island of Haparanda Hamn on 30-40 cm thick land-fast ice at a distance of about 100 m from the shoreline. The Finnish RV Aranda was placed in the ice-covered Bay of Bothnia inside the land-fast ice 15 km far from the nearest coast (Brümmer et al. 2003). Turbulent heat, radiation fluxes, moisture and momentum fluxes were measured as in BASIS 1998. The time interval of the measurements was 10 minutes at RV Aranda, 1 minute at Marjaniemi, and calculated values are again given at 6 hourly intervals.

6.2.1. Evolution of meteorological quantities

During BASIS 2001, the weather conditions were characterized by a rapid sequence of high- and low-pressure systems and passing atmospheric fronts. The time series of

the meteorological data pressure *p*, temperature *T*, water vapour mixing ratio *m*, wind speed *U* and wind direction *Wind Dir* at Marjaniemi and RV Aranda are shown in Figure 12. At the beginning of the experiment the weather was mild, but with the passage of a low on 21 February the wind backed from east to north, and the air temperature dropped to -20°C. Correspondingly, the water vapour mixing ratio fell to less than 1 gkg^{-1}. Generally, the comparison of measurements with extracted atmospheric (SMHI forcing) data at position Marjaniemi shows good agreement.

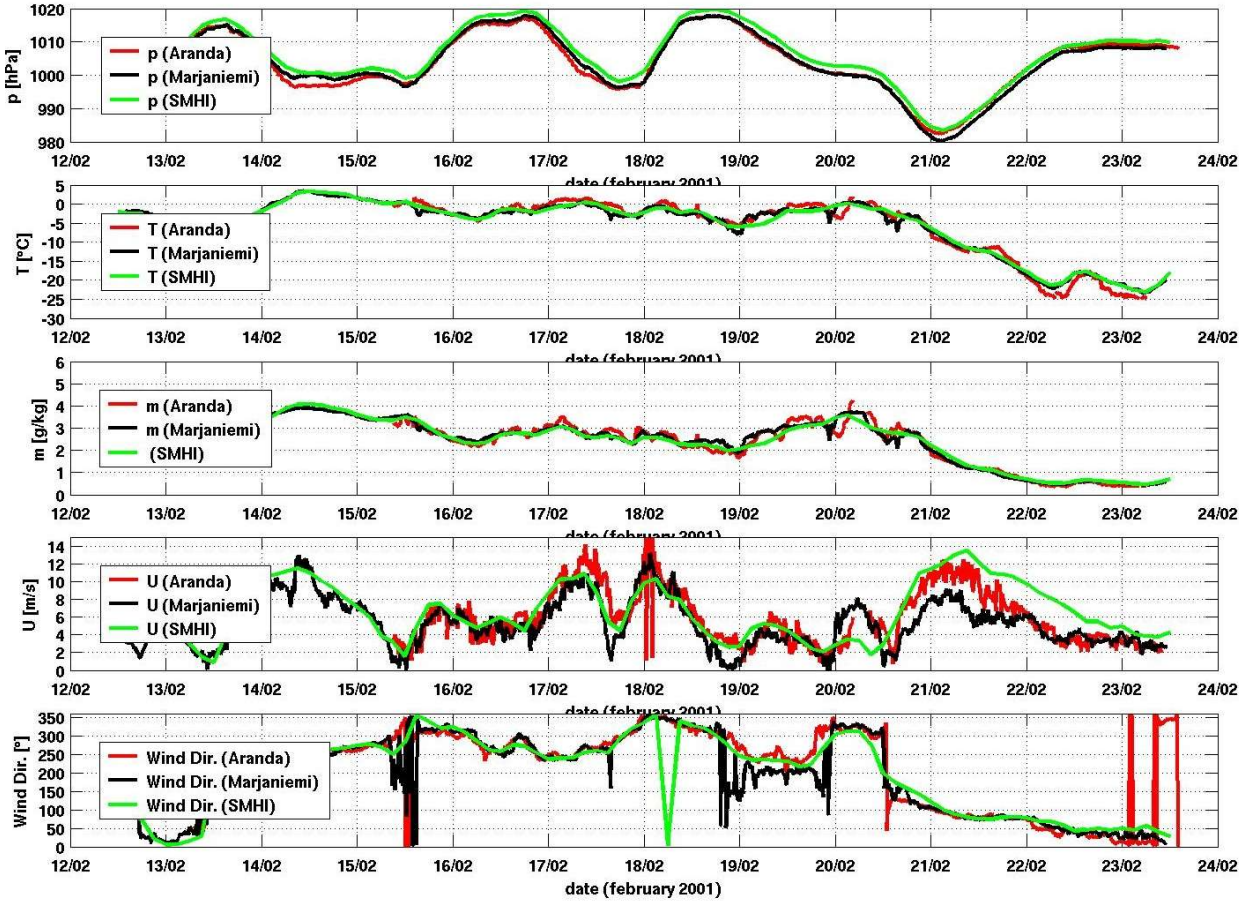

Figure 12. Time series of pressure *p*, temperature *T*, water vapour mixing ratio *m*, wind speed *U* and wind direction *Wind Dir.* at Marjaniemi and RV Aranda in comparison with observed atmospheric data at Marjaniemi.

6.2.2. Radiation fluxes

Radiation fluxes measured at Marjaniemi and RV Aranda are compared with calculated fluxes in Figure 13.

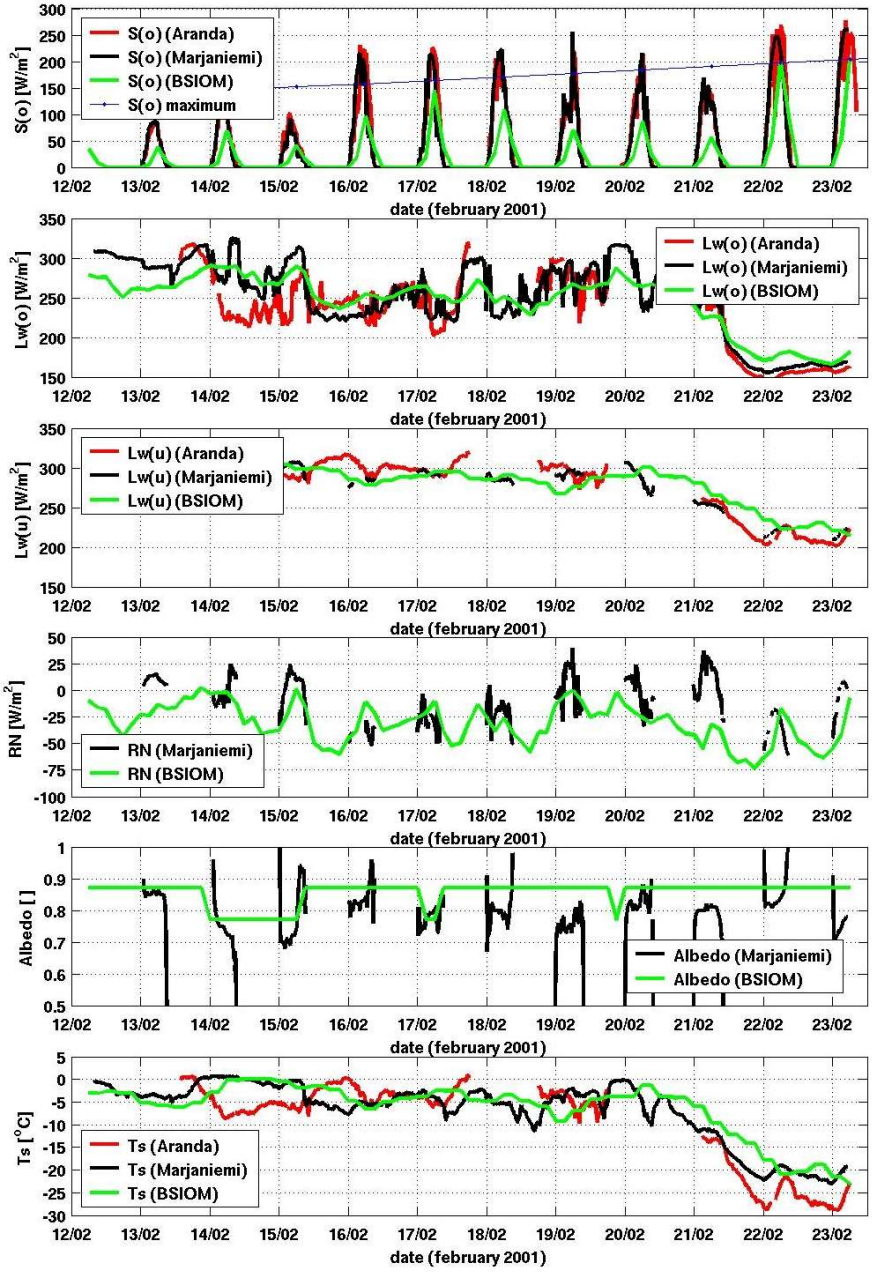

Figure 13. Time series of downwelling short-wave radiation *S(o)* (the blue line represents the daily clear sky *S(o)* maximum at Marjaniemi), downwelling long-wave radiation *Lw(o)*, upwelling long-wave radiation *Lw(u)*, net radiation *RN,* albedo and surface temperature T_s at Marjaniemi and RV Aranda in comparison with model data at Marjaniemi.

This shows that calculated the short-wave radiation is always less than the observed values. However, short-wave measurements overshoot the daily clear-sky maximum short-wave radiation, possibly because of reflection from clouds or snow over or inside the measurement instrument itself. Rapid changes in the incoming long-wave radiation *Lw(o)* indicate cloudiness. Extreme *Lw(o)* values were measured during

warm air periods with low-level clouds (e.g. about 300 Wm^{-2} on 14, 15 and 20 February) and during cold air periods with clear skies (e.g. 150 Wm^{-2} on 22 February). The measured upwelling long-wave radiation flux *Lw(u)* has many missing data, but calculated values (BSIOM) show nearly the same as the observations. The albedo of the land-fast ice at Marjaniemi varied depending on the weather conditions. Low values at the end of the melting periods (e.g., 15 February) and high albedo in cold periods, especially after a snow fall event. However, the modelled albedo show similar behaviour like the observed albedo.

The net radiation flux *RN* is only measured at Marjaniemi. The comparison reveals a good agreement in spite of data gapes. Little deviations are shown at the end of the campaign (e.g. 20, 21 February), because higher short-wave radiation at Kokkola conduct to discrepancies.

The structures of calculated *Lw(o)*, *Lw(u)*, *albedo*, *RN* and T_s are in good agreement with the measurements, despite the many gaps in the data.

6.2.3. Turbulent Fluxes

Turbulent surface fluxes are presented in Figure 14. The sensible heat flux *H* was only measured at RV Aranda. During the whole campaign, *H* was predominantly positive. That is a result of high wind speed and temperatures near melting point. The sensible and latent heat flux at Marjaniemi were calculated by bulk formulas according to equations 3.2 - 3.4. Especially for calculation *E* at RV Aranda the calculated surface temperature were used. The larger discrepancies between modelled heat fluxes and the measurements are due primarily to differences in SST and wind velocity.

The momentum flux shows three high periods (14, 17, 18 and 21, 22 February) which correlate well with periods of high wind speeds (Figure 12). The measured values are much higher than calculated data. The air-surface temperature difference $T\text{-}T_s$ shows nearly the same structure as the sensible heat flux, but the agreement between measured and calculated values shows higher discrepancies due to deviations in air and sea surface temperature.

All together considered, it is shown that measurements and calculations in BASIS 1998 are in better agreement than in BASIS 2001. Especially the radition fluxes in BASIS 2001 display larger differences.

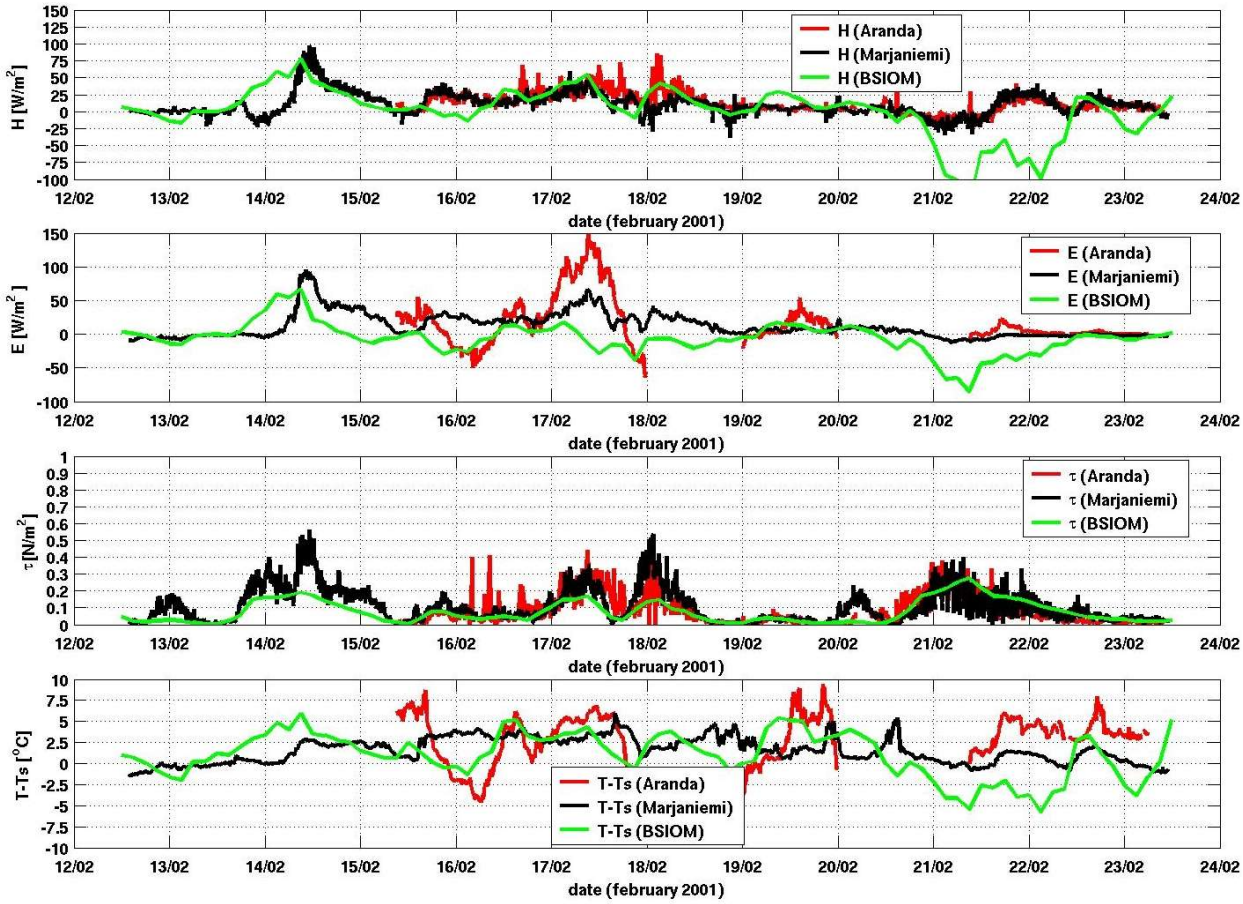

Figure 14. Time series of sensible heat flux H, latent heat flux E, momentum flux τ and air-surface temperature difference T-T_s at Marjaniemi and RV Aranda in comparison with model data at Marjaniemi.

6.3. Alkor 6/2001

The measurements of the BASIS experiments were performed at sea-ice; in contrast, the Alkor experiments were conducted over the open Baltic Sea. The position in the central Baltic Sea (56.02°N, 18.67°E, Figure 7) was chosen to sample data and to study in detail study the atmospheric and sea surface boundary layer at a purely marine location. This location is situated at the greatest distance from all coastlines. The nearest coast is the southern point of the island of Gotland at a distance of 110 km. The fetch for SW or NE winds is thus more than 300 km.

The hydrographic survey lasted from 12 to 20 June. Standard meteorological

quantities, turbulent heat, radiation and momentum fluxes were measured at the destination point in the central Baltic Sea from 13 to 19 June 2001. Turbulent heat and momentum fluxes were calculated by the same formula used in BSIOM (Equations 3.2 – 3.4).

6.3.1. Evolution of meteorological quantities

Synoptic weather conditions, pressure *p*, temperature *T*, water vapour mixing ratio *m*, wind speed *U* and wind direction *Wind Dir* are shown in Figure 15. The period was determined by slightly varying the surface pressure and slowly increasing the air temperature and humidity. However, wind speeds varied from strong to calm conditions.

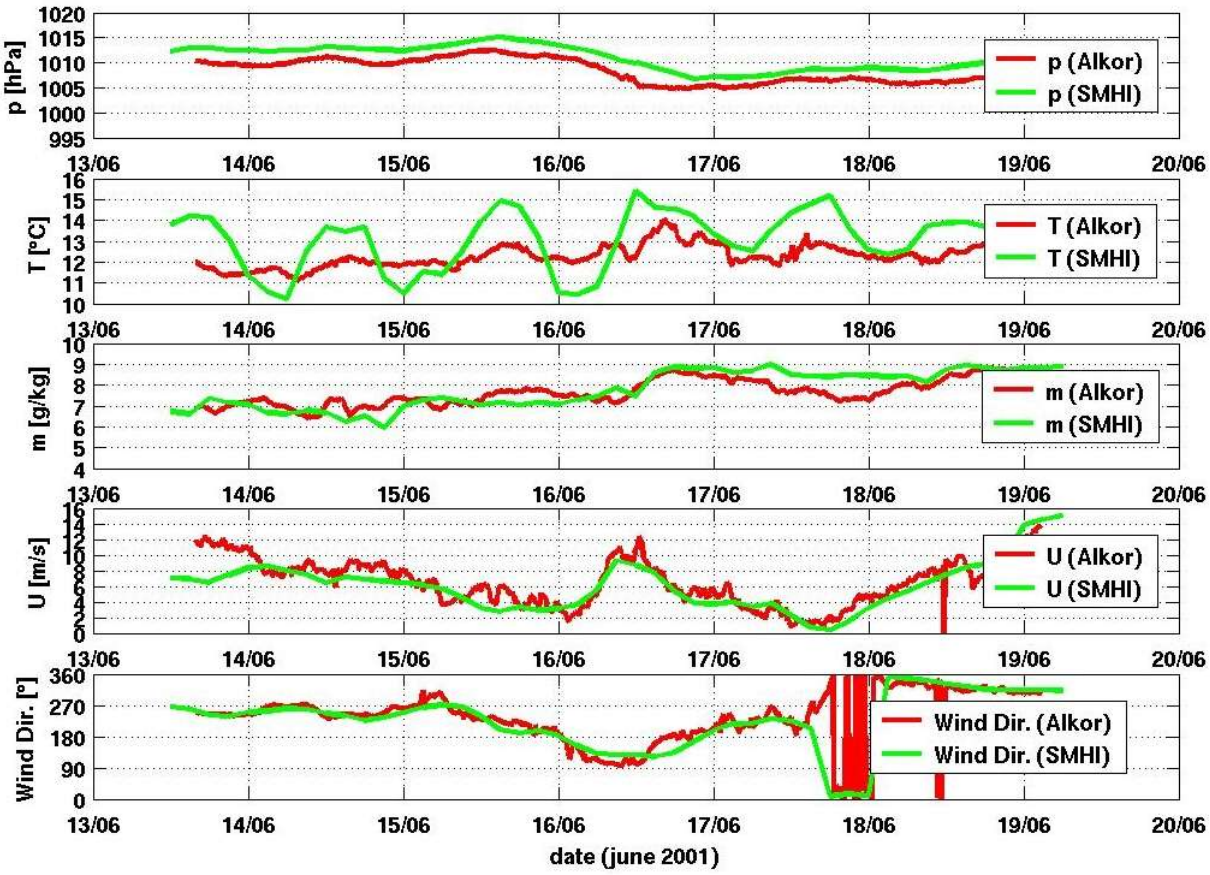

Figure 15. Time series of pressure *p*, temperature *T*, water vapour mixing ratio *m*, wind speed *U* and wind direction *Wind Dir* at RV Alkor in comparison with observed atmospheric data at position of RV Alkor (56.02°N, 18.67°E).

Extracted atmospheric (SMHI forcing) data at the Alkor position (56.02°N, 18.67°E) show a pronounced daily cycle in air temperature *T*. This clearly demonstrates a shortcoming of the SMHI-data. As mentioned in chapter 3, the database consists of synoptic measurements made on land. Temperature variations due to the daily cycle are thus extrapolated to the open sea. The air pressure *p* of the observed atmospheric data (SMHI) compares well with the RV Alkor measurements. The offset in air pressure results from different measurement heights. Calculated wind direction *Wind Dir* and wind speed *U* show good agreement with data from RV Alkor.

6.3.2. Radiation fluxes

The radiation fluxes *S(o)*, *Lw(o)*, *Lw(u)* as well as sea surface temperatures T_s are presented in Figure 16.

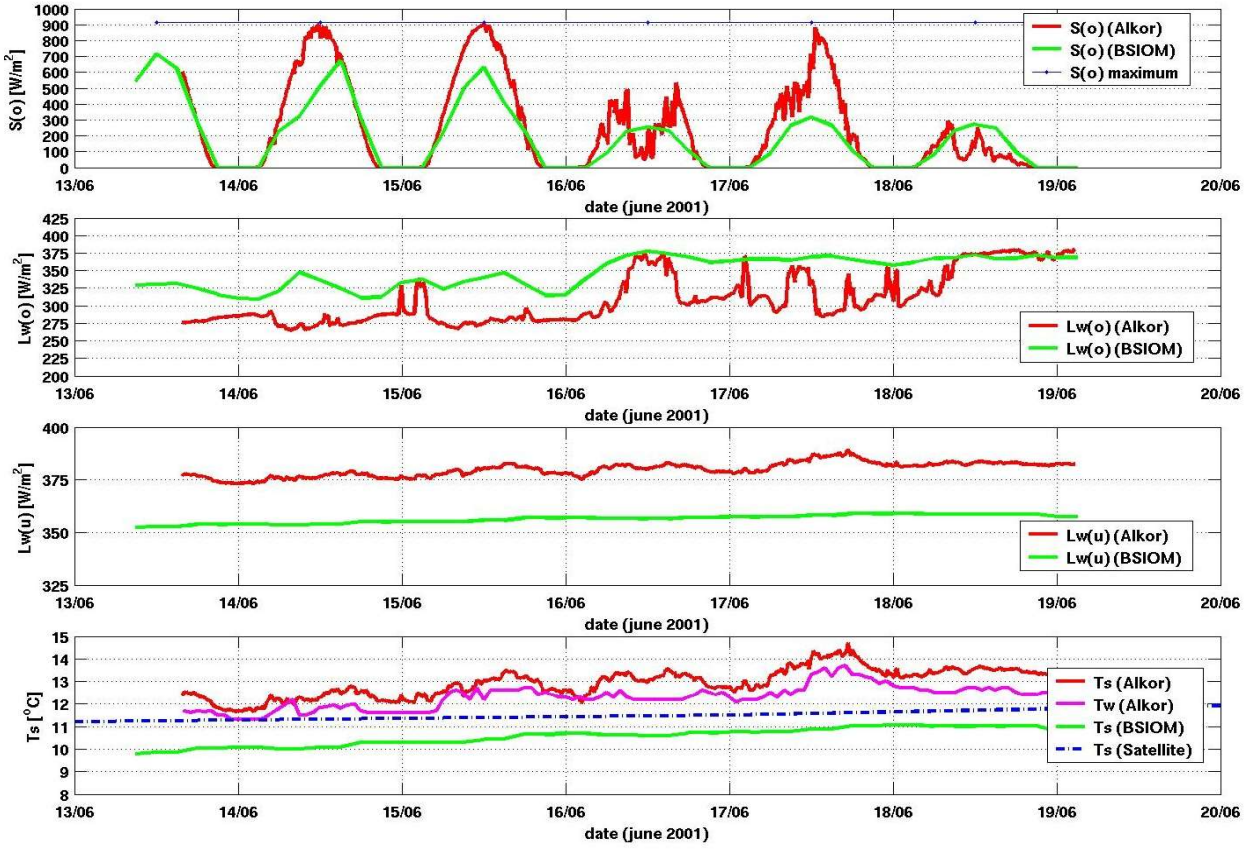

Figure 16. Time series of downwelling short-wave radiation *S(o)* (the blue line represents the daily clear sky *S(o)* maximum), downwelling long-wave radiation *Lw(o)*, upwelling long-wave radiation *Lw(u)*, surface temperature T_s and water temperature T_w at RV Alkor in comparison with model data at the position of Alkor (56.02°N, 18.67°E) and skin temperature from satellite.

The modelled short-wave radiation is generally less compared to the observations. The short-wave radiation *S(o)* shows often cloudfree conditions (14/15, 17 June), only on 16 and 18 June longer periods with cloud cover were observed. The incoming long-wave radiation flux reflects the cloudiness well. During cloudfree periods *Lw(o)* has a minimum and a maximum on cloudy days. The variability of the outgoing long-wave radiation *Lw(u)* is very small, because of the small variation of the sea surface temperature.
In spite of the generally good agreement of the meteorological parameters, radiation and SST reveal larger discrepancies. The modelled short-wave radiation is generally less compared to the observations.

6.3.3. Turbulent fluxes

Turbulent fluxes of heat and momentum are shown in Figure 17.

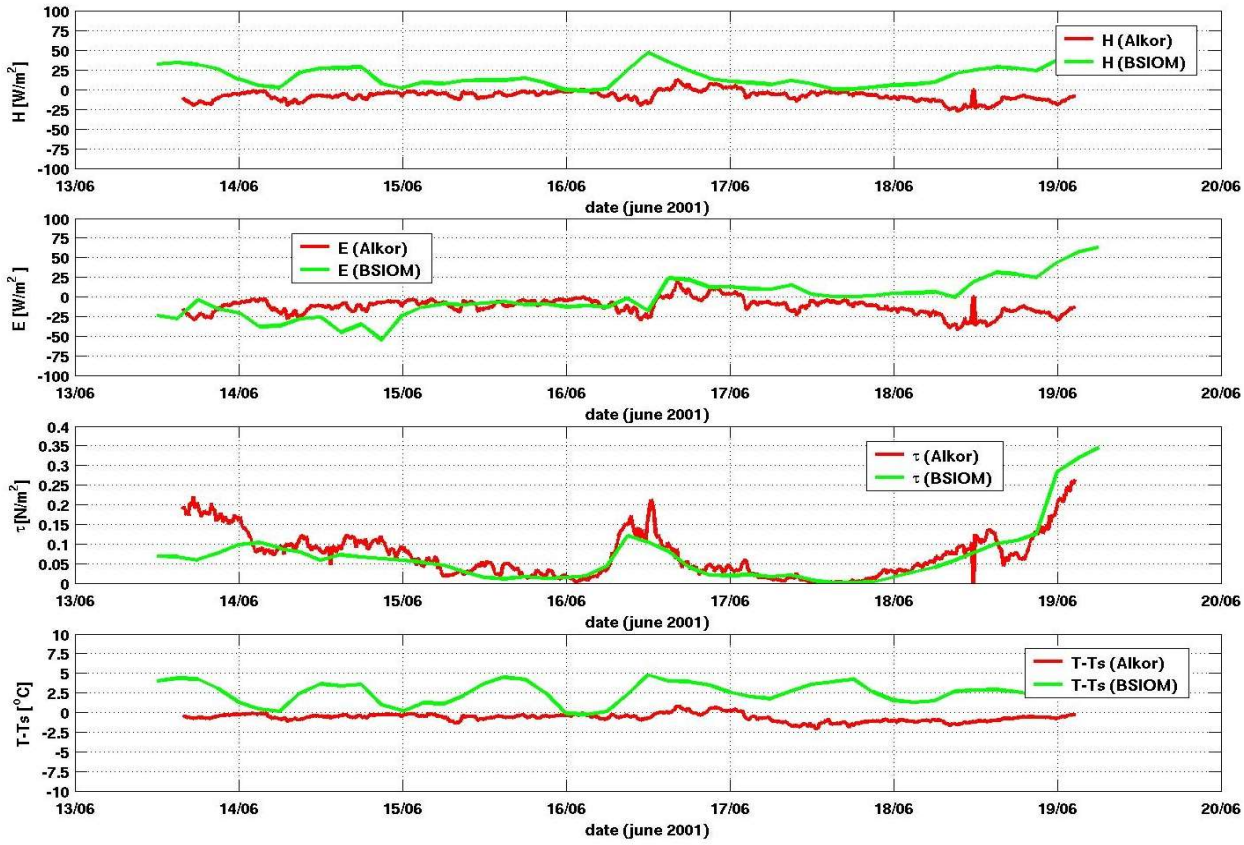

Figure 17. Time series of sensible heat flux *H*, latent heat flux *E*, momentum flux τ and air-surface temperature difference T-T_s at RV Alkor in comparison with model data at the position RV Alkor (56.02°N, 18.67°E).

For this experiment, no turbulent flux measurements have been conducted; fluxes were therefore calculated by bulk formulas according to Equations 3.2 - 3.4. As a result of the daily cycle of SMHI air temperatures and the differences in SST, the sensible heat flux is mainly negative for the 'measurements' and positive for BSIOM. Latent heat fluxes agree reasonably well, and wind stress calculations are strongly correlated.

Chapter 7

Statistical comparison of model estimates with measurements

In this section for the eight field experiments, a quantitative assessment of the quality of the atmospheric forcing and corresponding fluxes used in BSIOM is presented. For the statistical comparison of measurements with model estimates, daily mean values are used (Tables III-V). Further, long time series of meteorological data at Kiel lighthouse (Figure18) and IFM-GEOMAR (Figure 20) for the years 1998, 2000 and 2001 were used to support the statistics of the short timeseries of the field experiments, to determine the quality of the model data and to find systematical errors. Also here, monthly mean values and standard deviation were used for statistical comparison of measurements with model estimates (Attachment A, Tables VI, XI). A description of these gauging stations are presented in Table I and Table II.

Figure 18. Kiel Lighthouse (Maritime Meteorologie, IFM-GEOMAR).

Description of gauging station: Kiel Lighthouse

Position:	
Latitude	54°30' N
Longitude	10°16.5' E
Description of parameters and instruments:	
Wind direction [°] relative to North	Vane in 35m height above sea level
Wind speed [m/s]	Anemometer in 35m height above sea level
Air temperature [° C]	Thermometer in 35m height above sea level
relative Humidity [%]	moisture measuring device in 35m height above sea level
Water temperature [° C]	Water thermometer in 1.5m water depth (Pier Leuchtturm)
short-wave radiation [W/m²]	Solarimeter in 33,5m height above sea level measuring range: 0.3 - 2.8 µm

Table I. Description of of gauging station: Kiel Lighthouse (Maritime Meteorologie, IFM-GEOMAR).

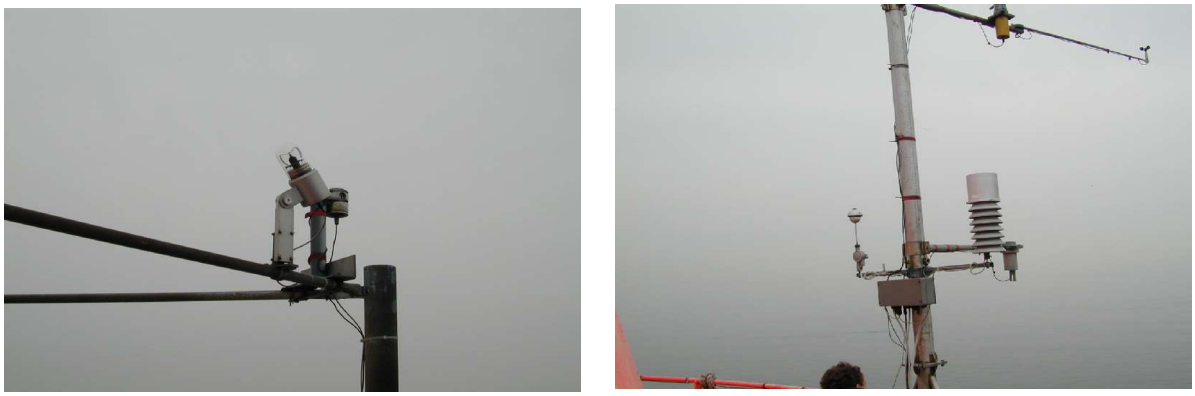

Figure 19. Left radiation measuring instrument and right moisture measuring device and thermometer at station Kiel lighthouse.

Description of gauging station: rooftop of IFM-GEOMAR

Figure 20. Gauging station at the rooftop of IFM-GEOMAR (Maritime Meteorologie, IFM-GEOMAR).

Position:	
Latitude	54°19.8' N
Longitude	10°9.0' E
Description of parameters and instruments:	
Wind direction [Grad] relative to North	Vane in 36m height above sea level
Wind speed [m/s]	Anemometer in 49.5m height above sea level
Air temperature [° C]	Thermometer in 34m height above sea level
relative Humidity [%]	moisture measuring device in 34m height above sea
Water temperature [° C]	Water thermometer in 0.2m water depth (Institute-Pier)
short-wave radiation [W/m²]	Solarimeter in 34,5m height above sea level measuring range: 0.3 - 2.8 µm
long-wave radiation [W/m²]	Pyrgeometer in 34,5m height above sea level measuring range: 4 - 50 µm
Air pressure [hPa] based on altitude	Barometer

Table II. Description of the gauging station at the rooftop of IFM-Geomar (Maritime Meteorologie, IFM-GEOMAR)

Generally, the comparison of measurements with extracted atmospheric (SMHI forcing) data at all positions shows good agreement. In particular, different air pressure estimates show the highest agreement for all experiments. Air temperatures and mixing ratios during winter experiments agree within less than 0.1°C and 0.05 gkg^{-1}, but over open water, the respective differences in temperature are about 0.04 °C in April 2000 and 2.65 °C in October 2000 as well as differences in moisture are about 0.12 gkg^{-1} in June 2001 and 0.65 gkg^{-1} in October 2001, owing to the daily cycle in the SMHI data. The measurements at Kiel lighthouse and IFM-GEOMAR differ in air temperature mean values to the extracted atmospheric (SMHI forcing) data between 0.01°C to 0.8°C (Attachment A, Table X, XI). But, in summer 2001 at station Kiel lighthouse larger differences with more than 1°C are found. Wind velocities agree within 2 ms^{-1} at Kiel stations, 1 ms^{-1} for the winter experiments, but for Kokkola the difference is about 4 ms^{-1} and for Alkor 4/2000 the difference is 3 ms^{-1}. The wind direction corresponds on average within 10° for the BASIS experiments. For the measurements at Kiel lighthouse and IFM-GEOMAR wind direction varied between 0.5° and 20°. Differences in wind speed and wind direction at Kiel stations could be traced back to differential measurement heights and the location of the measurement instruments. The surface temperatures at Kiel lighthouse vary between 0.09°C and 2°C which is probably due to the reduced solar insulation caused by greater cloud coverage. For the winter experiments surface temperatures agree within 1°C with a correlation coefficient of 0.9 and for Alkor experiments, the difference is about 2.5°C with the same reason. Further for the Alkor experiments, the correlation coefficients of T and m are smaller compared to the coefficients of the winter experiments. In general, simulated short-wave radiation fluxes are about 30 Wm^{-2} less than observations.

Long-wave radiation fluxes correspond within a few Wm^{-2} for the winter experiments, but for Alkor experiments and Kiel stations deviations are higher because of the differences in air and water temperatures.

For the comparison of turbulent fluxes, independent measurements exist for H and τ in BASIS 1998 and for H in BASIS 2001. Thus, any discrepancies between the remaining 'measured' and calculated fluxes depend on differences in the basic quantities; this has already been discussed. Sensible heat fluxes are well correlated with each other, but the differences between measured and calculated heat fluxes are about 4 and 1 Wm^{-2} for 1998, and 10 and 12 Wm^{-2} for February 2001 (Table III). Measured and calculated momentum fluxes display only small deviations and are strongly correlated with each other. This confirms the usability of the model for calculating surface winds and corresponding wind stresses from atmospheric surface pressure data (Bumke et al. 1998, Large & Pond, 1981).

BASIS 1998

	mean			Difference		standard deviation			corr.-coeff.		
	RV Aranda	**Kokkola**	**SMHI**	**Kokkola-SMHI**	**Aranda-SMHI**	**RV Aranda**	**Kokkola**	**SMHI**	**Kokk.-SMHI**	**Kokk.-Aranda**	**Aranda-SMHI**
p [hPa]	995.12	994.27	995.21	-0.94	-0.09	14.8	14.65	14.56	1	0.99	1
T [°C]	-4.35	-5.31	-5.32	0.01	0.97	5.96	6.48	6.56	0.98	0.93	0.98
m[gkg^{-1}]	2.59	2.41	2.37	0.04	0.22	1.15	1.03	1.12	0.98	0.95	0.99
U [ms^{-1}]	7.71	4.46	8.75	-4.29	-1.04	3.54	2.67	4.14	0.7	0.55	0.78
Wind Dir. [°]	198.11	196.05	210.1	-14.05	-11.99	94.12	84.75	96.53	0.77	0.64	0.68

	RV Aranda	**Kokkola**	**BSIOM**	**Kokkola-BSIOM**	**Aranda-BSIOM**	**RV Aranda**	**Kokkola**	**BSIOM**	**Kokk.-BSIOM**	**Kokk.-Aranda**	**Aranda-BSIOM**
S(o) [Wm^{-2}]	49.82	30.14	26.63	3.51	23.19	94.65	58.11	46.26	0.78	0.68	0.71
Lw(o) [Wm^{-2}]	260.34	253.13	257.66	-4.53	2.68	48.55	42.18	39.66	0.86	0.65	0.79
Lw(u) [Wm^{-2}]	279.62	278.05	279.49	-1.44	0.13	24.01	24.44	23.43	0.95	0.9	0.92
Ts [°C]	-8.35	-7.36	-6.35	-1.01	-2	5.78	5.93	5.71	0.91	0.91	0.92
H [Wm^{-2}]	10.07	6.96	11.08	-4.12	-1.01	19.8	23.51	24.48	0.92	0.6	0.69
E [Wm^{-2}]	-13.86	1.09	-9.23	10.32	-4.63	16.36	15.87	22.37	0.65	0.26	0.52
τ [Nm^{-2}]	0.11	0.1	0.14	-0.04	-0.03	0.12	0.12	0.13	0.5	0.63	0.84

BASIS 2001

	mean			Difference		standard deviation			corr.-coeff.		
	RV Aranda	**Marjaniemi**	**SMHI**	**Marj.-SMHI**	**Aranda-SMHI**	**RV Aranda**	**Marjaniemi**	**SMHI**	**Marj.-SMHI**	**Marj.-Aranda**	**Aranda-SMHI**
p [hPa]	1003.9	1003.8	1005.8	-2	-1.9	8.77	8.97	8.77	1	1	1
T [°C]	-6.31	-5.32	-5.39	0.07	-0.92	7.99	7.1	7.09	0.99	0.99	0.99
m[gkg^{-1}]	2.18	2.41	2.39	0.02	-0.21	0.98	0.99	0.99	0.99	0.98	0.98
U [ms^{-1}]	5.92	5.33	6.5	-1.17	-0.58	3.02	2.75	3.16	0.75	0.83	0.81
Wind Dir. [°]	213.31	189.83	192.96	-3.13	20.35	105.87	107.15	105.95	0.94	0.92	0.82

	RV Aranda	**Marjaniemi**	**BSIOM**	**Marj.-BSIOM**	**Aranda-BSIOM**	**RV Aranda**	**Marjaniemi**	**BSIOM**	**Marj.-BSIOM**	**Marj.-Aranda**	**Aranda-BSIOM**
S(o) [Wm^{-2}]	39.27	34.29	19.32	14.97	19.95	65.26	61.87	39.49	0.71	0.97	0.79
Lw(o) [Wm^{-2}]	230.35	252.05	246.1	5.95	-15.75	47.74	46.75	34.59	0.91	0.86	0.86
Lw(u) [Wm^{-2}]	275.56	278.92	279.35	-0.43	-3.79	36.78	27.38	23.65	0.9	0.92	0.91
Ts [°C]	-9.61	-6.87	-6.39	-0.48	-3.22	9.32	6.64	5.95	0.89	0.92	0.92
H [Wm^{-2}]	12.61	10.4	0.91	9.49	11.7	14.95	16.64	36.82	0.61	0.96	0.63
E [Wm^{-2}]	16.42	11.44	-6.23	17.67	22.65	37.79	18.19	23.11	0.58	0.52	0.21
τ [Nm^{-2}]	0.08	0.11	0.07	0.04	0.01	0.09	0.1	0.07	0.75	0.83	0.82

Table III. Statistical comparisons of model estimates and observations for BASIS 1998 and BASIS 2001.

Alkor 4/2000

	mean		difference	standard deviation		corr.-coeff.
	RV Alkor	**SMHI**	**Alkor-SMHI**	**RV Alkor**	**SMHI**	**Alkor-SMHI**
p [hPa]	1018.5	1021.1	-2.6	2.39	2.53	1
T [°C]	2.74	2.7	0.04	0.6	1.16	0.4
m[gkg^{-1}]	3.7	3.52	0.18	0.31	0.35	0.6
U [ms^{-1}]	7.36	4.73	2.63	3.17	1.67	0.84
Wind Dir. [°]	133.06	319.59	-186.53	348.93	68.17	-0.11

	RV Alkor	**BSIOM**	**Alkor-BSIOM**	**RV Alkor**	**BSIOM**	**Alkor-BSIOM**
S(o) [Wm^{-2}]	145.58	116.81	28.77	295.29	178.4	0.97
Lw(o) [Wm^{-2}]	268.84	281.38	-12.54	36.27	13.02	0.78
Lw(u) [Wm^{-2}]	328.53	327.31	1.22	2.84	0.33	-0.33
Ts [°C]	3.18	4.59	-1.41	0.58	0.07	-0.24
H [Wm^{-2}]	-5.54	-17.52	11.98	12.71	13.17	0.18
E [Wm^{-2}]	-4.58	-40.51	35.93	10.43	17.79	0.3
τ [Nm^{-2}]	0.09	0.04	0.05	0.06	0.02	0.79

Alkor 6/2000

	mean		difference	standard deviation		corr.-coeff.
	RV Alkor	**SMHI**	**Alkor-SMHI**	**RV Alkor**	**SMHI**	**Alkor-SMHI**
p [hPa]	1017.4	1019.6	-2.2	6.66	6.64	1
T [°C]	11.95	11.75	0.2	0.74	2.8	0.14
m[gkg^{-1}]	6.33	5.99	0.34	0.4	0.9	0.56
U [ms^{-1}]	6.82	5.34	1.48	3.07	2.27	0.76
Wind Dir. [°]	267.52	270.11	-2.59	62.15	46.48	0.5

	RV Alkor	**BSIOM**	**Alkor-BSIOM**	**RV Alkor**	**BSIOM**	**Alkor-BSIOM**
S(o) [Wm^{-2}]	307.77	217.12	90.65	327.11	230.19	0.97
Lw(o) [Wm^{-2}]	287.88	327.12	-39.24	23.5	20.01	0.42
Lw(u) [Wm^{-2}]	374.67	352.05	22.62	3.94	1.59	0.4
Ts [°C]	12.6	9.69	2.91	0.56	0.32	0.69
H [Wm^{-2}]	-8.37	14.16	-22.53	10.76	15.61	-0.48
E [Wm^{-2}]	-11.85	-28.38	16.53	15.34	20.77	0.46
τ [Nm^{-2}]	0.08	0.05	0.03	0.06	0.03	0.75

Alkor 10/2000

	mean		difference	standard deviation		corr.-coeff.
	RV Alkor	**SMHI**	**Alkor-SMHI**	**RV Alkor**	**SMHI**	**Alkor-SMHI**
p [hPa]	1007.9	1008.1	-0.2	4.96	5.3	0.9
T [°C]	10.44	7.79	2.65	1.14	2.01	0.27
m[gkg^{-1}]	6.48	5.9	0.58	1.05	0.86	0.03
U [ms^{-1}]	8.31	7.92	0.39	3.02	3.65	0.82
Wind Dir. [°]	241.51	239.77	1.74	63.8	46.56	0.02

	RV Alkor	**BSIOM**	**Alkor-BSIOM**	**RV Alkor**	**BSIOM**	**Alkor-BSIOM**
S(o) [Wm^{-2}]	31.75	26.54	5.21	64.76	46.18	0.69
Lw(o) [Wm^{-2}]	327.93	323.38	4.55	19.62	5.85	-0.12
Lw(u) [Wm^{-2}]	366.83	352.44	14.39	5.85	1.17	0.27
Ts [°C]	12.01	9.77	2.24	0.45	0.24	0.12
H [Wm^{-2}]	-25.52	-28.71	3.19	12.36	53.6	0.18
E [Wm^{-2}]	-34.87	-74.8	39.93	16.47	62.77	0.3
τ [Nm^{-2}]	0.11	0.21	-0.1	0.07	0.18	0.79

Table IV. Statistical comparisons of model estimates and observations at station Alkor/2000.

Alkor 4/2001

	mean		difference	standard deviation		corr.-coeff.
	RV Alkor	**SMHI**	**Alkor-SMHI**	**RV Alkor**	**SMHI**	**Alkor-SMHI**
p [hPa]	1006.6	1009.1	-2.5	4.37	4.46	1
T [°C]	4.71	6.17	-1.46	0.97	1.71	0.43
m[gkg^{-1}]	4.79	4.95	-0.16	0.3	0.48	0.85
U [ms^{-1}]	7.45	7.1	0.35	2.49	2.96	0.78
Wind Dir. [°]	200.33	204.7	-4.37	49.02	43.64	0.92

	RV Alkor	**BSIOM**	**Alkor-BSIOM**	**RV Alkor**	**BSIOM**	**Alkor-BSIOM**
S(o) [Wm^{-2}]	165.24	94.9	70.34	225.68	135.92	0.94
Lw(o) [Wm^{-2}]	282.39	304.83	-22.44	35.34	16.65	0.66
Lw(u) [Wm^{-2}]	335.63	327.11	8.52	1.67	0.57	0.35
Ts [°C]	4.22	4.54	-0.32	0.35	0.12	0.35
H [Wm^{-2}]	10.83	13.81	-2.98	16.32	17.36	0.49
E [Wm^{-2}]	10.31	-10.41	20.72	15.5	15.91	0.07
τ [Nm^{-2}]	0.09	0.08	0.01	0.06	0.08	0.79

Alkor 6/2001

	mean		difference	standard deviation		corr.-coeff.
	RV Alkor	**SMHI**	**Alkor-SMHI**	**RV Alkor**	**SMHI**	**Alkor-SMHI**
p [hPa]	1008.3	1010.9	-2.6	2.35	2.39	0.97
T [°C]	12.29	13.05	-0.76	0.54	1.38	0.6
m[gkg^{-1}]	7.65	7.77	-0.12	0.62	0.9	0.8
U [ms^{-1}]	6.47	6.1	0.37	2.95	3.19	0.9
Wind Dir. [°]	233.15	225.09	8.06	75.25	83.16	0.8

	RV Alkor	**BSIOM**	**Alkor-BSIOM**	**RV Alkor**	**BSIOM**	**Alkor-BSIOM**
S(o) [Wm^{-2}]	232.18	193.26	38.92	274.07	211.47	0.59
Lw(o) [Wm^{-2}]	309.34	347.57	-38.23	35.68	22.16	0.69
Lw(u) [Wm^{-2}]	379.9	356.32	23.58	3.33	1.95	0.76
Ts [°C]	12.94	10.55	2.39	0.63	0.39	0.76
H [Wm^{-2}]	-8.19	16.74	-24.93	6.54	13.22	0.32
E [Wm^{-2}]	-12.17	-2.24	-9.93	9.83	24.72	0.07
τ [Nm^{-2}]	0.07	0.07	0	0.06	0.07	0.89

Alkor 10/2001

	mean		difference	standard deviation		corr.-coeff.
	RV Alkor	**SMHI**	**Alkor-SMHI**	**RV Alkor**	**SMHI**	**Alkor-SMHI**
p [hPa]	1005.9	1010.8	-4.9	10.74	11.58	0.98
T [°C]	9.1	8.86	0.24	1.85	2.34	0.86
m[gkg^{-1}]	6.11	5.46	0.65	1.14	1.6	0.8
U [ms^{-1}]	15.1	15.22	-0.12	3.88	3.99	0.68
Wind Dir. [°]	274.45	270.35	4.1	34.98	27.44	0.92

	RV Alkor	**BSIOM**	**Alkor-BSIOM**	**RV Alkor**	**BSIOM**	**Alkor-BSIOM**
S(o) [Wm^{-2}]	57.13	37.31	19.82	96.33	59.22	0.91
Lw(o) [Wm^{-2}]	308.76	316.44	-7.68	34.16	21.4	0.6
Lw(u) [Wm^{-2}]	362.05	344.51	17.54	3.71	0.86	0.78
Ts [°C]	9.52	8.17	1.35	0.72	0.18	0.78
H [Wm^{-2}]	-12.92	10.65	-23.57	43.04	49.6	0.74
E [Wm^{-2}]	-8.31	-79.57	71.26	47.25	99.87	0.03
τ [Nm^{-2}]	0.34	0.38	-0.04	0.17	0.18	0.72

Table V. Statistical comparisons of model estimates and observations at station Alkor/2001.

Chapter 8

Discussion

Besides temporal and spatial variability, the differences in meteorological quantities result from the different measurement methods with different accuracies, as well as from the distance between measurement stations and the locations of the instrumentations. For example the SMHI database includes surface pressure, 2-m air temperature, 2-m relative humidity and geostrophic wind whereas the locations of measurements at RV Aranda are 11 m for pressure, air temperature and humidity, the wind speed and direction were measured at 19 m height. Further, the values at Kiel lighthouse and IFM-GEOMAR were measured in 34 m height and higher above sea level. The differences in spite of the distance between measurement stations is especially evident in BASIS 1998 for the stations Kokkola and RV Aranda, which lay some 80 km apart (Figure 7). Moreover, the measurements at Kiel lighthouse are more significant than the measurements at IFM-GEOMAR, due to the location, because the position near the coast are less influenced by land than the station in town.

The accuracy of extracted atmospheric data (SMHI forcing) is determined by the accuracy of the underlying synoptic measurements and of the interpolation method for extrapolating land-based measurements to the open sea. Independent measurements near the coast generally compare well with extracted atmospheric data (SMHI forcing) (Figure 8 and 12), but over the open sea, a spurious daily cycle in T is apparent, which is clearly a shortcoming of the SMHI database (Figure 15).

In spite of the generally good agreement of the basic meteorological quantities, larger differences appear in radiation fluxes. The calculated $S(o)$ is always less than the measurements, but between the stations Kokkola and RV Aranda (1998) larger differences also occur, which are due to regional distinctions, and differences in

cloud cover. The largest differences in S(o) are shown in spring and summer at Kiel lighthouse with differences in mean values up to 50 Wm^{-2}. One reason for this behaviour might be the difference in cloud cover between coast and open sea. Even on these times convective clouds are present, which are local effects and difficult to model. Differences in solar radiation could also be the reason for the excessively low simulated sea surface temperatures in Alkor experiments. SSTs derived from satellite data taken from weekly SST maps provided by the BSH (Bundesamt für Seeschiffahrt und Hydrographie in Hamburg, Germany), lie between KT19 skin temperature measurements (Brümmer et al. 2003) and simulated data (Figure 16). But there may also be other reasons for the differences in surface temperatures. The advection of air masses plays an important role, as well as the short-wave radiation. Furthermore, if there is ice, the ice fraction and thickness will be required for calculating ice temperatures.

SSTs are the result of the development of the surface energy balance and turbulent mixing in the ocean, so seasonal development has to be taken into account when comparing temperatures. A bias in cloud coverage can thus lead to intermittent and locally greater differences in SST development. Furthermore, measurement methods or measurement errors (e.g. measurement height, the perspective of KT19 or precipitation) can cause larger differences, which is especially shown at RV Alkor, where the water surface temperature was measured by an Infrared radiometer KT19 at the upper deck of the ship in about 9 m height and modelled T_s represent the water temperature at 1.5 m depth. Further, it can be shown that during cloudfree conditions and warm air advection the water surface temperature rise, but in deeper water the temperature react very slowly and delayed. Also during light wind conditions a diurnal thermocline may change the surface temperature by a few degrees. The satellite temperature lies between the water surface temperature of RV Alkor and the calculated temperature and represents that the values of BSIOM are not unrealistic (Figure 16, 17).

The accuracy of the calculated surface fluxes depends on the quality of the observations and on bulk aerodynamic formulas used to calculate them. The bulk method is a practicable way to estimate surface fluxes, but the determination of the corresponding drag and transfer coefficients introduces an uncertainty to this method. Drag and transfer coefficients depend on the stability of the planetary boundary layer, wind waves and swell. Additionally, the drag coefficient is sensitive to water depth, whereas heat transfer coefficients are not expected to be as sensitive to limitations in water depth (Rutgersson et al. 2001). Generally, the sensitivity with respect to small variations in wind velocity is expected to be small, but slight effects due to high winds cannot be ruled out (De Cosmo et al. 1996, Makin 1998). The

validity of transfer coefficients has been investigated in a number of studies (e.g. Large & Pond 1982, Smith 1988, 1989, Rutgersson et al. 2001), which claim that the main uncertainty arises from measurement errors or inaccurate measurements. In particular, the determination of the stanton number C_H is highly sensitive to surface temperature measurement errors (e.g. Calanca 2001, Schröder et al. 2003). Thus, calculated heat fluxes are always encumbered with systematic errors, and larger discrepancies in measured and calculated data result not only from differences in meteorological quantities, but also from uncertainties in transfer coefficients; e.g. Rutgersson et al. (2001), for example, found that a 10% uncertainty in the heat transfer coefficient results in 10 Wm^{-2} uncertainty in heat fluxes. Furthermore, measurement errors in sensible and latent heat fluxes of about 15 and 30 Wm^{-2}, respectively, are related to a difference of 1°C in air-sea temperature and humidity of 1 gkg^{-1}. For calculated fluxes this kind of accuracy is hard to achieve.

To assess the validity of the bulk formula used to calculated sensible heat fluxes, 'measured' and calculated heat fluxes were compared, for which measured basic meteorological quantities were used (Table XII). The difference between 'measured' and calculated fluxes are well within the expected range of uncertainty (Rutgersson et al. 2001).

Döscher et al. (2002) compared monthly mean heat fluxes averaged over the Baltic Sea area with heat fluxes obtained from a regional coupled ocean-atmosphere model. They found maximum differences of up to 15 Wm^{-2} for sensible heat fluxes, and up to 50 Wm^{-2} for latent heat fluxes, which are close to differences obtained in this study.

	mean	mean	Difference	standard deviation		corr.-coeff.	corr.-coeff.
1998	**Kokkola** (measured)	**Kokkola** (calculated)	**Kokkola (m)-Kokkola (c)**	**Kokkola** (measured)	**Kokkola** (calculated)	**Kokk. (m)-Kokkola (c)**	**BSIOM-Kokkola (c)**
H [Wm^{-2}]	6.96	24.2	-17.24	23.51	32.59	0.79	0.65
2001	**Marjaniemi** (measured)	**Marjaniemi** (calculated)	**Marj. (m)-Marj. (c)**	**Marjaniemi** (measured)	**Marjaniemi** (calculated)	**Marj. (m)-Marj. (m)**	**BSIOM-Marjaniemi (c)**
H [Wm^{-2}]	10.4	18.13	-7.73	16.64	19.84	0.77	0.5

Table XII. Comparison of measured and calculated sensible heat fluxes.

Chapter 9

Summary and conclusions

Observed basic meteorological quantities, heat and radiation fluxes from three different measurement stations in the Baltic Sea are compared with model data of the coupled sea-ice-ocean model BSIOM in order to evaluate the atmospheric forcing, corresponding surface fluxes and the sea surface response. Further, a statistical comparison of meteorological quantities, radiation fluxes and heat fluxes of the BALTIMOS experiments with calculated model data has been carried out. Above all, long timeperiods of Kiel institute and Kiel lighthouse for the years 1998, 2000 and 2001 were utilised to evaluate statistically the atmospheric forcing of the coupled sea ice-ocean model BSIOM.

Observational data were made available from the BASIS winter campaigns in 1998 and 2001, from the RV Alkor cruises in 2000 and 2001 as well as from the Kiel stations in 1998, 2000 and 2001. Generally, observed basic meteorological quantities and model data are in good agreement. However, measurements over sea-ice correspond better with the model than measurements over open water, mainly because of a spurious daily cycle in the air temperature of the SMHI database. Observations at Kiel lighthouse and IFM-GEOMAR compare well with the atmospheric forcing.

The simulated short-wave radiation is generally less than the observed values; this is due to uncertainties in the prescribed cloud coverage, also provided by the SMHI data. These uncertainties are reflected in water temperature and upwelling long-wave radiation. The long time series of Kiel lighthouse near the coast and IFM-GEOMAR reinforce the problem of short-wave radiation as well as the uncertainties in water temperature and upwelling long-wave radiation.

Turbulent flux measurements were conducted only for the sensible heat and momentum flux for the winter experiments in 1998 and 2001. Calculated sensible

heat fluxes correlate well with observations, even though the mean difference range from 4 to 12 Wm^{-2}. Comparison of measured fluxes and fluxes calculated with the bulk method using observed basic meteorological quantities displays a high correlation with an uncertainty of 7-17 Wm^{-2}, which is well within the expected range of uncertainty given by Rutgersson et al. (2001). Hence, the bulk formula used to calculate the sensible heat fluxes provides good estimates in comparison with the measurements. Furthermore, the correspondence between measured and calculated momentum fluxes is very high, which in turn confirms the usability of the model component to calculate surface winds and wind stresses from atmospheric surface pressure. Accordingly, the approach (equations 3.2-3.6) seems to be well suited to calculate the heat and energy exchange between the ocean, sea-ice and atmosphere.

It has been demonstrated that measurements such as the BALTIMOS field campaigns are extremely useful for validation of coupled model systems. The time series are relatively short, however; that is to say, the statistical analysis of surface fluxes has a somewhat low significance. Additionally, the representativeness of measurements for a larger area needs to assessed. Döscher et al. (2002) compared heat flux observations averaged over the area of the Baltic Sea with heat fluxes obtained from a regional coupled ocean-atmosphere model. For my knowledge, however, the present study is the first to have validated a sophisticated coupled sea-ice-ocean model with the aid of directly measured atmospheric parameters and fluxes over sea- ice and open water.

Further, for a better quantification of the energy and water cycle of the Baltic area a detailed evaluation of sophisticated models must include not only the standard parameters but also the fluxes; this must therefore involve a detailed analysis of coupling mechanisms and forcing functions. Hence, longer flux measurements at the air-sea-ice interface and air-sea interface are needed to improve the understanding of the information exchange between ocean and atmosphere. With such a detailed validation the reliability of coupled model systems will increase and uncertainties will be reduced.

Attachment A

Appendix to Chapter 7

Kiel-Leuchtturm (SMHI) 1998

	mean											
	Jan	**Feb**	**Mar**	**Apr**	**May**	**Jun**	**Jul**	**Aug**	**Sep**	**Oct**	**Nov**	**Dec**
p [hPa]	1013.3	1018.8	1017.9	1004.5	1015.9	1013.3	1009.3	1014.4	1010.8	1007.3	1016.9	1015.9
	standard deviation											
	14.76	9	12.12	7.79	8.57	5	5.33	6.69	13.2	10.97	12.39	11.04
	mean											
T [°C]	3.55	5.3	4.96	7.51	12.43	15.21	15.37	15.89	13.97	9.26	2.65	1.69
	standard deviation											
	3.11	3.52	3.3	2.72	3.18	2.79	2.65	2.7	2.31	2.27	3.18	3.92
	mean											
m[gkg^{-1}]	4.41	5	4.42	5.73	7.13	8.73	8.91	8.95	8.63	6.2	4.17	3.99
	standard deviation											
	1.08	1.19	1.32	1.07	1.31	1.61	1.25	1.19	1.27	1.26	1.05	1.18
	mean											
U [ms^{-1}]	7.37	10	7.38	5.37	5.85	5.12	6.44	6.15	5.21	10.48	5.54	8.23
	standard deviation											
	3.95	3.32	3.52	2.42	2.4	3.15	3.61	2.77	3.03	3.99	2.75	3.96
	mean											
Wind Dir. [°]	196.96	247.02	226.78	150.01	170.54	204.41	227.33	241.32	147.07	195.83	191.85	218.46
	standard deviation											
	87.79	30.65	74.23	76.91	105.56	75.66	60.51	75.8	72.66	74.38	93.92	64.14
	mean											
Ts[°C]	4.59	4.36	5.83	8.17	13.83	16.48	16.79	16.99	15.91	12.26	7.55	3.62
	standard deviation											
	0.46	1.03	0.37	0.98	1.65	0.59	0.4	0.54	0.35	1.49	1.41	0.68
	mean											
Sw [W/m²]	18.34	27.25	74.26	88.12	190.04	167.3	156.02	137.72	74.28	46.7	22.85	13.69
	standard deviation											
	38.02	43.2	113.27	113.82	217.16	176.82	164.84	157.67	101.48	72.31	41.16	31.52
	mean											
Lw [W/m²]	295.16	312.16	299.37	322.85	336.64	365.49	365.91	365.38	363.16	328.03	291.5	285.55
	standard deviation											
	24.22	27.15	27.74	20.38	22.61	23.12	19.57	23.64	20.52	24.56	23.34	28.99

Kiel-Leuchtturm (SMHI) 2000

	mean											
	Jan	**Feb**	**Mar**	**Apr**	**May**	**Jun**	**Jul**	**Aug**	**Sep**	**Oct**	**Nov**	**Dec**
p [hPa]	1017.9	1013.3	1014.7	1008.7	1015.7	1017.1	1009.8	1016.8	1014.6	1011.2	1003.3	1008.3
	standard deviation											
	10.25	9.88	9.39	10.04	7.44	4.76	6.67	3.54	7.27	10.7	7.34	10.96
	mean											
T [°C]	3.3	4.37	4.76	8.5	13.2	14.71	15.11	16.35	13.9	11.5	7.27	4.7
	standard deviation											
	2.79	2.3	1.98	4.17	3.47	4.37	2.47	2.61	2.3	2.26	1.74	4.32
	mean											
m[gkg^{-1}]	4.35	4.67	4.74	5.89	7.1	8.19	8.87	9.31	8.44	7.55	5.73	5.03
	standard deviation											
	1	0.74	0.85	1.62	1.01	1.89	1.27	1.41	1.43	1.03	0.62	1.51
	mean											
U [ms^{-1}]	9.92	9.3	8.46	4.65	5.13	6.01	5.62	4.29	5.62	6.8	7.53	7.01
	standard deviation											
	4.66	4.09	4.73	2.43	3.35	3.2	2.64	2.04	2.83	4	2.72	3.83
	mean											
Wind Dir. [°]	246.71	237.05	222.86	182.26	166.92	230.03	242.74	231.88	173.19	178.67	177.98	178.74
	standard deviation											
	59.18	54.96	97.66	91.6	95.03	75.72	92.23	67.9	79.19	43.58	27.64	70.83
	mean											
Ts[°C]	3.57	4.08	4.65	6.78	13.35	15.43	16.14	18.14	16.7	13.84	9.38	7.19
	standard deviation											
	0.36	0.22	0.41	1.43	1.44	0.88	0.58	0.4	0.96	1.09	1	1.04
	mean											
Sw [W/m²]	17.4	34.07	58.52	116.09	210.95	190.26	155.83	148.09	89.13	54.98	22.98	11.92
	standard deviation											
	36.35	56.95	88.01	153.8	240.98	210.6	170.64	171.47	126.5	91.54	40.51	25.38
	mean											
Lw [W/m²]	295.28	300.32	304.77	319.91	337.46	356.74	365.14	366.68	357.09	339.02	316.63	303.37
	standard deviation											
	22.39	21.05	20.27	27.63	23	25.61	17.22	23.46	24.12	20.8	17.09	28.93

Kiel-Leuchtturm (SMHI) 2001

	mean											
	Jan	**Feb**	**Mar**	**Apr**	**May**	**Jun**	**Jul**	**Aug**	**Sep**	**Oct**	**Nov**	**Dec**
p [hPa]	1013.4	1015.6	1007.2	1010.4	1017.2	1014.2	1014.5	1016.8	1008.5	1014.1	1017	1019.3
	standard deviation											
	14.28	13.78	8.13	7.2	7.63	5.76	6.68	5.62	6.49	7.12	11.12	18.98
	mean											
T [°C]	2.01	1.84	2.31	6.39	12.19	13.52	17.99	17.88	13.11	12.98	6.08	1.42
	standard deviation											
	2.68	3.76	3.58	3	3.3	3.22	3.12	3.15	1.75	2.28	2.91	2.78
	mean											
m[gkg^{-1}]	4.13	3.97	3.95	5.07	6.82	7.84	10.31	10.37	8.3	8.25	5.11	3.84
	standard deviation											
	0.85	1.18	1.22	1.14	1.19	1.58	1.58	1.89	0.78	1.19	1.18	0.89
	mean											
U [ms^{-1}]	5.77	7.08	6.63	5.77	5.07	5.2	4.42	5.27	5.91	7.49	8.16	6.95
	standard deviation											
	3.12	3.65	3.49	2.63	2.81	2.88	2.41	3.06	3.68	3.6	3.74	4.35
	mean											
Wind Dir. [°]	184.79	213.84	152.42	198.89	198.94	235.75	195.91	194.3	199.2	187.52	251.05	222.34
	standard deviation											
	82.62	99.71	87.45	90.34	122	89.23	100.12	75.5	92.56	54.84	68.47	104.27
	mean											
Ts[°C]	4.08	2.82	2.57	4.43	10	14	18.28	18.6	16.19	14.08	9.17	5.01
	standard deviation											
	0.79	0.28	0.33	0.79	2.08	0.9	0.93	0.72	1.16	0.67	1.67	1.41
	mean											
Sw [W/m²]	14.93	35.71	69.3	109.57	203.23	173.29	199.59	152.55	79.13	50.42	26.49	12.32
	standard deviation											
	29.48	57.35	108.67	139.82	227.37	180.57	218.75	175.99	110.3	78.46	47.38	26.38
	mean											
Lw [W/m²]	290.38	286.78	287.95	308.16	332.19	351.95	375.94	377.25	355.7	349.96	306.62	283.45
	standard deviation											
	19.26	24.92	28.49	23.11	24.31	23.72	20.3	25.51	17.13	19.57	27.87	22.53

Table VI. Statistical values of model estimates at station Kiel lighthouse for 1998, 2000 and 2001.

Kiel-Leuchtturm 1998

	mean Jan	Feb	Mar	Apr	May	Jun	Jul	Aug	Sep	Oct	Nov	Dec
p [hPa]												
	standard	deviation										
	mean											
T [°C]	3.81	5.17	4.83	7.82	13.22	15.94	16.13	16.25	14.03	9.56	3.2	1.99
	standard											
	2.96	3.39	3.07	2.83	3.13	2.63	2.81	2.59	1.73	2.17	2.99	3.91
	mean											
m[gkg^{-1}]												
	standard	deviation										
	mean											
U [ms^{-1}]	8.29	10.15	8.18	7.01	6.57	5	7.7	7.81	5.99	11.14	6.95	8.43
	standard	deviation										
	4.09	2.97	3.41	3.45	3.36	3.5	3.46	2.85	4.38	3.56	2.92	4.23
	mean											
Wind Dir. [°]	177.46	241.65	219.55	151.88	172.56	203.28	227.39	235.49	150.36	199.24	179.99	221.88
	standard	deviation										
	86.33	35.73	84.66	83.54	108.3	80.33	66.28	80.64	74.99	67.88	89.73	61.61
	mean											
Ts[°C]	3.3	3.51	4.59	6.22	11.75	15.14	16.08	16.86	14.93	11.3	6.8	2.87
	standard	deviation										
	0.9	0.91	0.33	1.2	1.45	0.89	0.55	0.65	0.47	1.06	1.66	0.64
	mean											
Sw [W/m²]	24.74	37.55	108.64	108.96	220.92	200.71	187.31	179.1	87.49	52.38	26.05	16.58
	standard	deviation										
	55.62	76.26	173.78	173.29	266.26	253.78	237.34	234.71	146.02	102.72	58.28	41.03
	mean											
Lw [W/m²]												
	standard	deviation										

Kiel-Leuchtturm 2000

	mean Jan	Feb	Mar	Apr	May	Jun	Jul	Aug	Sep	Oct	Nov	Dec
p [hPa]												
	standard	deviation										
	mean											
T [°C]	3.94	4.97	5.17	8.94	12.7	14.56	14.82	16.54	14.02	11.7	7.63	4.99
	standard	deviation										
	2.51	2.18	1.97	3.39	2.82	4.05	1.89	1.91	1.82	1.91	1.7	4.07
	mean											
m[gkg^{-1}]												
	standard	deviation										
	mean											
U [ms^{-1}]	9.93	9.62	8.49	5.44	6.43	7.12	6.47	6.01	7.68	8.19	8.68	8.29
	standard	deviation										
	3.83	3.6	4.25	3.31	3.68	3.48	2.5	2.41	3.1	3.74	2.37	3.31
	mean											
Wind Dir. [°]	234.36	228.55	212.76	173.17	169.36	224.43	229.07	220.3	170.29	186.44	186.31	193.04
	standard	deviation										
	65.4	60.48	100.72	88.94	90.82	76.55	90	77.31	77.09	42.48	30.26	66.04
	mean											
Ts[°C]	3.43	3.29	3.95	6.32	12.13	14.59	15.5	17.26	14.97	12.54	9.17	6.99
	standard	deviation										
	0.44	0.18	0.51	1.44	1.51	1.39	0.85	0.38	1.27	0.6	0.87	1.2
	mean											
Sw [W/m²]	22.53	44.74	83.55	150.5	239.21	217.91	183.17	176.36	103.1	57.65	27.74	16.1
	standard	deviation										
	53.44	90.97	145.85	213.84	285.15	265.05	242.18	232.66	164.4	105.31	57.65	39.11
	mean											
Lw [W/m²]												
	standard	deviation										

Kiel-Leuchtturm 2001

	mean Jan	Feb	Mar	Apr	May	Jun	Jul	Aug	Sep	Oct	Nov	Dec
p [hPa]												
	standard	deviation										
	mean											
T [°C]	2.34	1.99	1.73	6.08	11.71	13.03	16.83	16.23	12.17	12.52	5.64	0.72
	standard	deviation										
	2.52	3.72	2.32	2.87	2.88	2.63	2.28	2.55	1.38	2.32	2.2	2.5
	mean											
m[gkg^{-1}]												
	standard	deviation										
	mean											
U [ms^{-1}]	6.83	8.14	8.16	7.13	6.01	6.4	6.13	6.95	7.14	8.28	8.78	7.96
	standard	deviation										
	2.87	3.33	3.68	2.83	3.28	2.67	2.88	3.03	3.31	3.19	3.15	3.31
	mean											
Wind Dir. [°]	180.6	199.83	144.35	195.67	187.57	226.2	192.16	193.76	204.4	188.51	235.43	200.03
	standard	deviation										
	71.48	98.36	84.84	89.34	113.19	91.65	93.56	80.63	83.92	52.76	80.99	104.81
	mean											
Ts[°C]	3.92	2.42	2.48	4.54	10.7	13.94	18.37	18.34	15.46	13.39	9.02	5.13
	standard	deviation										
	0.58	0.26	0.55	0.87	2.35	1.45	1.46	0.85	1.28	0.6	1.6	3
	mean											
Sw [W/m²]	19.6	52.19	113.46	137.42	250.61	224.13	222.44	175.82	96.37	60.32	31.52	14.6
	standard	deviation										
	46.03	100.78	176.47	201.91	295.5	274.74	270.94	230.59	160.33	109.68	65.48	35.55
	mean											
Lw [W/m²]												
	standard	deviation										

Table VII. Statistical values of observations at station Kiel lighthouse for 1998, 2000 and 2001.

Kiel-Institut (SMHI) 1998

	mean											
	Jan	**Feb**	**Mar**	**Apr**	**May**	**Jun**	**Jul**	**Aug**	**Sep**	**Oct**	**Nov**	**Dec**
p [hPa]	1013.4	1018.9	1017.9	1004.4	1015.9	1013.3	1009.3	1014.4	1010.8	1007.4	1016.9	1016
	standard	**deviation**										
	14.74	8.99	12.09	7.78	8.54	5	5.31	6.68	13.18	10.91	12.39	11.01
	mean											
T [°C]	3.57	5.31	4.99	7.56	12.47	15.24	15.39	15.91	13.94	9.25	2.64	1.69
	standard	**deviation**										
	3.12	3.56	3.33	2.73	3.22	2.81	2.67	2.74	2.33	2.3	3.21	3.96
	mean											
RH [%]	89.53	90.62	82.31	90.25	83.32	85.48	86.41	84.64	91.17	87.29	90.52	91.64
	standard	**deviation**										
	9.42	9.29	14.59	10.35	12.17	12.28	10.49	10.78	8.13	9.16	7.5	7.68
	mean											
U [ms^{-1}]	6.28	7.97	6.27	4.84	4.87	4.38	5.37	5.1	4.69	8.69	4.82	7
	standard	**deviation**										
	3.3	2.53	2.91	2.25	2.01	2.59	2.9	2.27	2.83	3.29	2.33	3.15
	mean											
Wind Dir. [°]	198.34	242.59	223.77	149.69	168.45	203.16	225.28	240.64	144.95	192.21	190.85	215.45
	standard	**deviation**										
	86.65	30.33	73.29	77.6	105.66	74.24	58.75	72.97	72.02	73.77	92.91	62.81
	mean											
Ts[°C]												
	standard	**deviation**										
	mean											
Sw [W/m²]	18.41	27.36	74.18	88.28	189.87	167.03	155.92	137.65	74.3	46.77	22.94	13.77
	standard	**deviation**										
	38.09	43.34	113.25	114.14	217.14	176.58	164.66	157.63	101.35	72.48	41.25	31.58
	mean											
Lw [W/m²]	295.28	312.16	299.57	323.07	336.86	365.73	366.03	365.48	363.1	328.04	291.46	285.54
	standard	**deviation**										
	24.25	27.31	27.85	20.5	22.79	23.22	19.66	23.7	20.65	24.62	23.48	29.14

Kiel-Institut (SMHI) 2000

	mean											
	Jan	**Feb**	**Mar**	**Apr**	**May**	**Jun**	**Jul**	**Aug**	**Sep**	**Oct**	**Nov**	**Dec**
p [hPa]	1018	1013.4	1014.8	1008.7	1015.7	1017.1	1009.8	1016.8	1014.6	1011.2	1003.3	1008.3
	standard	**deviation**										
	10.25	9.88	9.39	10.04	7.44	4.76	6.67	3.54	7.27	10.7	7.34	10.96
	mean											
T [°C]	3.29	4.39	4.79	8.55	13.25	14.76	15.13	16.38	13.92	11.5	7.27	4.69
	standard	**deviation**										
	2.81	2.32	2	4.21	3.51	4.4	2.48	2.64	2.3	2.28	1.76	4.35
	mean											
RH [%]	90.93	91.51	90.51	85.91	79.98	82.54	87.41	85.66	89.61	93.03	92.22	93.09
	standard	**deviation**										
	9.63	7.17	9.15	11.81	14.03	13.11	10.08	12.46	10.75	7.04	5.57	5.81
	mean											
U [ms^{-1}]	8.15	7.67	6.92	4.15	4.4	5.02	4.64	3.57	5.09	6.17	7.07	6.15
	standard	**deviation**										
	3.79	3.29	3.85	2.2	2.84	2.63	2.2	1.74	2.63	3.59	2.56	3.18
	mean											
Wind Dir. [°]	244.38	233.45	222	182.87	163.99	228.17	240.48	228.8	172.93	177.12	177.06	179.13
	standard	**deviation**										
	56.85	54.06	96.14	90.74	94.9	74.24	90.94	67.09	78.05	42.72	27.02	70.41
	mean											
Ts[°C]												
	standard	**deviation**										
	mean											
Sw [W/m²]	17.45	34.15	58.46	116.11	210.77	190.16	155.76	147.95	89.08	55.06	23.06	11.97
	standard	**deviation**										
	36.46	56.99	87.82	153.82	241.03	210.69	169.75	171.23	126.53	91.56	40.65	25.42
	mean											
Lw [W/m²]	295.25	300.39	305.02	320.13	337.03	357.03	365.37	366.87	357.22	339.03	316.57	303.34
	standard	**deviation**										
	22.47	21.11	20.33	27.88	23.1	25.71	17.28	23.59	24.28	20.93	17.19	29.04

Kiel-Institut (SMHI) 2001

	mean											
	Jan	**Feb**	**Mar**	**Apr**	**May**	**Jun**	**Jul**	**Aug**	**Sep**	**Oct**	**Nov**	**Dec**
p [hPa]	1013.4	1015.6	1007.2	1010.4	1017.2	1014.2	1014.5	1016.8	1008.5	1014.1	1017	1019.3
	standard	**deviation**										
	14.28	13.78	8.13	7.2	7.63	5.76	6.68	5.62	6.49	7.12	11.12	18.98
	mean											
T [°C]	1.99	1.86	2.35	6.43	12.34	13.55	18.02	17.9	13.1	12.98	6.07	1.41
	standard	**deviation**										
	2.7	3.79	3.59	3.03	3.33	3.24	3.14	3.18	1.76	2.3	2.92	2.78
	mean											
RH [%]	94.27	90.2	86.32	85.98	81.17	84.93	85.6	86.38	92.76	92.7	88.86	91.31
	standard	**deviation**										
	3.76	7.85	10.89	12.16	12.81	11.22	11.68	11.83	7.77	6.58	8.96	7.59
	mean											
U [ms^{-1}]	5.23	5.99	5.74	4.99	4.2	4.29	3.8	4.53	4.98	6.5	6.67	5.81
	standard	**deviation**										
	2.98	3.12	2.97	2.21	2.3	2.36	2.1	2.56	3.1	2.84	2.99	3.58
	mean											
Wind Dir. [°]	184.18	212.19	151.17	200.72	163.99	198.71	238.39	1195.88	191.58	197.38	185.32	222.88
	standard	**deviation**										
	81.59	98.57	87.9	88.72	121.62	84.61	98.92	74.34	91.25	53.36	64.62	101.98
	mean											
Ts[°C]												
	standard	**deviation**										
	mean											
Sw [W/m²]	14.99	35.7	69.11	109.48	203.05	172.77	199.17	152.37	78.95	50.46	26.48	12.37
	standard	**deviation**										
	29.54	57.28	108.38	139.65	227.33	179.93	218.32	175.87	109.95	78.55	47.33	26.41
	mean											
Lw [W/m²]	290.3	287.23	288.23	308.38	332.47	352.21	376.13	377.45	355.76	350.02	306.7	283.52
	standard	**deviation**										
	19.35	25.05	28.53	23.23	24.44	23.81	20.36	25.59	17.17	19.67	27.9	22.54

Table VIII. Statistical values of model estimates at station IFM-GEOMAR for 1998, 2000, 2001.

Kiel-Institut 1998

	Jan	Feb	Mar	Apr	May	Jun	Jul	Aug	Sep	Oct	Nov	Dec
	mean											
p [hPa]	1012.38	1017.95	1017.11	1003.89	1015.06	1012.28	1007.92	1012.8	1010.9	1007.02	1016.38	1015.08
	standard deviation											
	14.73	9.31	11.68	7.66	8.61	5.09	5.16	6.63	13.15	10.72	12.24	10.92
	mean											
T [°C]	4.33	5.91	5.67	8.44	12.93	15.47	15.66	15.96	14.24	9.37	2.96	2.05
	standard deviation											
	3.27	3.73	3.86	3.27	3.38	3	3.11	3.19	2.19	2.47	3.18	4.41
	mean											
RH [%]	89.52	89.4	73.76	80.73	72.07	74.75	76.32	74.8	83.6	83.38	87.89	89.57
	standard deviation											
	11.02	11.02	17.98	14.15	14.38	14.81	14.14	13.63	10.63	10.17	9.33	9.77
	mean											
U [ms^{-1}]	5.2	5.41	5.09	4.74	4.63	4.05	4.33	4.13	4.18	6.17	3.96	4.97
	standard deviation											
	2.65	1.68	2.36	2.2	2.2	1.84	1.77	1.62	2.43	2.59	1.5	2
	mean											
Wind Dir. [°]	180.07	238.05	219.55	146.98	154.84	200.26	221.58	228.06	141.86	191.16	186.45	213.6
	standard deviation											
	82.77	35.24	79.4	86.27	111.02	78.23	66.43	76.01	75.61	68.7	83.22	59.43
	mean											
Ts[°C]	3.98	3.66	5.31	7.59	01/03/93	15.14	15.56	17.14	15.41	11.79	7.35	4.01
	standard deviation											
	0.53	0.82	0.87	1.37	1.63	1.02	1.16	0.93	0.7	1.23	1.7	1.43
	mean											
Sw [W/m²]	23.22	35.09	104.65	106.33	212.79	183.8	178.68	165.38	82.49	48.73	26.12	15.8
	standard deviation											
	54.92	73.21	171.87	172.16	261.3	238.09	228.15	219.22	135.87	97.46	57.61	38.79
	mean											
Lw [W/m²]	312.11	332.57	309.53	343.33	349.62	380.31	381.72	377.15	379.61	341.13	309.68	301.45
	standard deviation											
	38.33	40.99	46.72	30.9	34.73	32.66	29.4	33.13	27.36	38.16	37.72	47.22

Kiel-Institut 2000

	Jan	Feb	Mar	Apr	May	Jun	Jul	Aug	Sep	Oct	Nov	Dec
	mean											
p [hPa]	1017.2	1012.36	1014.21	1008.34	1014.87	1015.64	1009.19	1015.64	1013.85	1010.8	1004.24	1007.59
	standard deviation											
	10.13	9.91	9.09	10.12	7.33	5.07	6.81	3.62	7.52	11.13	7.22	10.91
	mean											
T [°C]	3.68	4.92	5.09	9.84	13.81	15.46	15.46	16.65	13.88	11.09	7.13	4.52
	standard deviation											
	2.86	2.5	2.25	4.78	3.84	4.94	2.55	2.82	2.43	2.26	1.82	1.97
	mean											
RH [%]	87.64	87.82	87.65	79.39	71.24	73.19	78.03	75.82	82.87	83.51	83.81	84.96
	standard deviation											
	1	0.74	0.85	1.62	1.01	1.89	1.27	1.41	1.43	1.03	0.62	1.51
	mean											
U [ms^{-1}]	5.52	5.57	5.32	4.08	4.31	4.42	3.83	3.39	4.59	4.88	5.42	4.94
	standard deviation											
	2.4	2.31	2.68	2.01	2.33	1.75	1.51	1.7	2.39	2.64	1.82	1.97
	mean											
Wind Dir. [°]	232.19	226.67	206.39	163.92	148.68	220.63	330.4	219.77	164.18	180.56	182.91	188.59
	standard deviation											
	62.45	56.34	100.84	87.69	93.13	77.79	92.94	75.83	75.83	44.74	29.72	61.7
	mean											
Ts[°C]	3.93	4.04	5.08	8.14	13.99	14.55	15.95	17.49	15.48	13.31	10.01	7.19
	standard deviation											
	0.59	0.31	0.83	2.4	2.38	1.62	1.33	0.65	1.18	0.78	1.03	1.45
	mean											
Sw [W/m²]	20.44	41.86	75.56	149.61	231.22	208.99	166.02	170.23	101.29	56.95	25.95	15.49
	standard deviation											
	50.13	87.82	138.33	214.57	272.73	257.76	223.13	224.6	165.18	105.63	53.93	36.47
	mean											
Lw [W/m²]	315.7	319.09	326.11	337.07	348.23	377.66	381.49	373.47	365.89	345.31	322.9	313.61
	standard deviation											
	38.18	35.46	36.31	39.02	33.98	33.05	26.28	33.96	34.02	31.27	31.46	40.82

Kiel-Institut 2001

	Jan	Feb	Mar	Apr	May	Jun	Jul	Aug	Sep	Oct	Nov	Dec
	mean											
p [hPa]	1012.96	1015.08	1011	1009.95	1016.79	1013.75	1012.78	1012.93	1008.2	1014	1017.15	1020.01
	standard deviation											
	14.11	13.79	9.4	7.14	7.93	5.62	6.68	5.51	6.57	7.25	10.85	18.31
	mean											
T [°C]	1.87	2.09	2.01	7.11	12.83	13.9	18.2	17.89	12.49	12.74	5.7	0.13
	standard deviation											
	2.9	4.08	2.94	3.65	3.49	3.49	3.25	3.55	1.79	2.55	2.86	3.04
	mean											
RH [%]	88.34	84.54	77.47	78.75	71.45	77.51	78.22	80.08	89.78	88.01	86.81	89.49
	standard deviation											
	5.9	10.32	12.43	14.27	15.42	13.51	12.74	13.51	9.34	8.05	10.52	10.31
	mean											
U [ms^{-1}]	4.15	4.85	5.52	4.42	3.95	3.7	3.7	3.75	3.76	4.62	4.19	4.04
	standard deviation											
	1.95	2.14	3.02	1.8	2.06	1.63	1.9	1.97	2.15	1.97	1.8	2.19
	mean											
Wind Dir. [°]	174.1	198.12	143.01	188.09	165.45	225.79	177.72	186.1	199.82	184.18	235.18	210.76
	standard deviation											
	68.83	97.22	83.31	89.4	117.83	90.17	94.65	79.2	79.6	53.67	69.04	95.71
	mean											
Ts[°C]	4.52	3.31	3.37	5.75	11.69	14.69	17.89	19.41	15.83	14.05	9.57	5.02
	standard deviation											
	0.95	0.85	0.76	1.07	2.05	1.49	2.51	1.11	1.43	0.57	1.77	1.9
	mean											
Sw [W/m²]	17.82	50.15	110.58	124.88	241	201.16	210.53	174.33	87.54	59.13	31.03	13.57
	standard deviation											
	40.97	98.78	173.81	188.36	289.15	253.43	259.12	229.18	145.88	106.92	65.75	32.46
	mean											
Lw [W/m²]	304.07	300.04	279.1	319.54	338.59	363.89	384.08	381.75	362.1	353.9	310	296.12
	standard deviation											
	34.12	37.24	41.48	38.81	35.43	31.28	28.39	33.86	26.71	29.02	44.92	39.11

Table IX. Statistical values of observations at station IFM-GEOMAR for 1998, 2000 and 2001.

Lighthouse

Differences 1998

	Jan	Feb	Mar	Apr	May	Jun	Jul	Aug	Sep	Oct	Nov	Dec
p [hPa]												
T [°C]	0.26	-0.13	-0.13	0.31	0.79	0.73	0.76	0.36	0.06	0.3	0.55	0.3
RH [%]	0.34	-0.82	-2.86	-8.07	-11.01	-12.86	-12.82	-10.7	-4.8	-2.51	-2.23	-1.4
U [ms^{-1}]	0.92	0.15	0.8	1.64	0.72	-0.12	1.26	1.66	0.78	0.66	1.41	0.2
Wind Dir. [°]	-19.5	-5.37	-7.23	1.87	2.02	-1.13	0.06	-5.83	3.29	3.41	-11.86	3.42
Ts[°C]	-1.29	-0.85	-1.24	-1.95	-2.08	-1.34	-0.71	-0.13	-0.98	-0.96	-0.75	-0.75
Sw [W/m²]	6.4	10.3	34.38	20.84	30.88	33.41	31.29	41.38	13.21	5.68	3.2	2.89
Lw [W/m²]												

Differences 2000

	Jan	Feb	Mar	Apr	May	Jun	Jul	Aug	Sep	Oct	Nov	Dec
p [hPa]												
T [°C]	0.64	0.6	0.41	0.44	-0.5	-0.15	-0.29	0.19	0.12	0.2	0.36	0.29
RH [%]	-3.94	-4.24	-3.86	-4.44	-6.27	-5.46	-4.49	-7.42	-5.75	-6.65	-6.18	-4.57
U [ms^{-1}]	0.01	0.32	0.03	0.79	1.3	1.11	0.85	1.72	2.06	1.39	1.15	1.28
Wind Dir. [°]	-12.35	-8.5	-10.1	-9.09	2.44	-5.6	-13.67	-11.58	-2.9	7.77	8.33	14.3
Ts[°C]	-0.14	-0.79	-0.7	-0.46	-1.22	-0.84	-0.64	-0.88	-1.73	-1.3	-0.21	-0.2
Sw [W/m²]	5.13	10.67	25.03	34.41	28.26	27.65	27.34	28.27	13.97	2.67	4.76	4.18
Lw [W/m²]												

Differences 2001

	Jan	Feb	Mar	Apr	May	Jun	Jul	Aug	Sep	Oct	Nov	Dec
p [hPa]												
T [°C]	0.33	0.15	-0.58	-0.31	-0.48	-0.49	-1.16	-1.65	-0.94	-0.46	-0.44	-0.7
RH [%]	-2.24	-2.95	-6.23	-0.44	-3.29	-3.66	-4.94	-6.93	-8.13	-8.44	-7.95	-6.22
U [ms^{-1}]	1.06	1.06	1.53	1.36	0.94	1.2	1.71	1.68	1.23	0.79	0.62	1.01
Wind Dir. [°]	-4.19	-14.01	-8.07	-3.22	-11.37	-9.55	-3.75	-0.54	5.2	0.99	-15.62	-22.31
Ts[°C]	-0.16	-0.4	-0.09	0.11	0.7	-0.06	0.09	-0.26	-0.73	-0.69	-0.15	0.12
Sw [W/m²]	4.67	16.48	44.16	27.85	47.38	50.84	22.85	23.27	17.24	9.9	5.03	2.28
Lw [W/m²]												

Table X. Differences of mean values between model estimates and observation values at station Kiel lighthouse for 1998, 2000 and 2001.

IFM-GEOMAR

Differences 1998

	Jan	Feb	Mar	Apr	May	Jun	Jul	Aug	Sep	Oct	Nov	Dec
p [hPa]	-1.02	-0.95	-0.79	-0.51	-0.84	-1.02	-1.38	-1.6	0.1	-0.38	-0.52	-0.92
T [°C]	0.76	0.6	0.68	0.88	0.46	0.23	0.27	0.05	0.3	0.12	0.32	0.36
RH [%]	-0.01	-1.22	-8.55	-9.52	-11.25	-10.73	-10.09	-9.84	-7.57	-3.91	-2.63	-2.07
U [ms^{-1}]	-1.08	-2.56	-1.18	-0.1	-0.24	-0.33	-1.04	-0.97	-0.51	-2.52	-0.86	-2.03
Wind Dir. [°]	-18.27	-4.54	-4.22	-2.71	-13.61	-2.9	-3.7	-12.58	-3.09	-1.05	-4.4	-1.85
Ts[°C]												
Sw [W/m²]	4.81	7.73	30.47	18.05	22.92	16.77	22.76	27.73	8.19	1.96	3.18	2.03
Lw [W/m²]	16.83	20.41	9.96	20.26	12.76	14.58	15.69	11.67	16.51	13.09	18.22	15.91

Differences 2000

	Jan	Feb	Mar	Apr	May	Jun	Jul	Aug	Sep	Oct	Nov	Dec
p [hPa]	-0.8	-1.04	-0.59	-0.36	-0.83	-1.46	-0.61	-1.16	-0.75	-0.4	0.94	-0.71
T [°C]	0.39	0.53	0.3	1.29	0.56	0.7	0.33	0.27	-0.04	-0.41	-0.14	-0.17
RH [%]	-3.29	-3.69	-2.86	-6.52	-8.74	-9.35	-9.38	-9.84	-6.74	-9.52	-8.41	-8.13
U [ms^{-1}]	-2.63	-2.1	-1.6	-0.07	-0.09	-0.6	-0.81	-0.18	-0.5	-1.29	-1.65	-1.21
Wind Dir. [°]	-12.19	-6.78	-15.61	-18.95	-15.31	-7.54	89.92	-9.03	-8.75	3.44	5.85	9.46
Ts[°C]												
Sw [W/m²]	2.99	7.71	17.1	33.5	20.45	18.83	10.26	22.28	12.21	1.89	2.89	3.52
Lw [W/m²]	20.45	18.7	21.09	16.94	11.2	20.63	16.12	6.6	8.67	6.28	6.33	10.27

Differences 2001

	Jan	Feb	Mar	Apr	May	Jun	Jul	Aug	Sep	Oct	Nov	Dec
p [hPa]	-0.44	-0.52	3.8	-0.45	-0.41	-0.45	-1.72	-3.87	-0.3	-0.1	0.15	0.71
T [°C]	-0.12	0.23	-0.34	0.68	0.49	0.35	0.18	-0.01	-0.61	-0.24	-0.37	-1.28
RH [%]	-5.93	-5.66	-8.85	-7.23	-9.72	-7.42	-7.38	-6.3	-2.98	-4.69	-2.05	-1.82
U [ms^{-1}]	-1.08	-1.14	-0.22	-0.57	-0.25	-0.59	-0.1	-0.78	-1.22	-1.88	-2.48	-1.77
Wind Dir. [°]	-10.08	-14.07	-8.16	-12.63	1.46	27.08	-60.67	-9.78	8.24	-13.2	49.86	-12.12
Ts[°C]												
Sw [W/m²]	2.83	14.45	41.47	15.4	37.95	28.39	11.36	21.96	8.59	8.67	4.55	1.2
Lw [W/m²]	13.77	12.81	-9.13	11.16	6.12	11.68	7.95	4.3	6.34	3.88	3.3	12.6

Table XI. Differences of mean values between model estimates and observation values at station IFM-GEOMAR for 1998, 2000 and 2001.

References

Anderson, R. J., 1987. Wind stress measurements over rough ice during the 1884 Marginal Ice Zone Experiment. J. Geophys. Res., Vol. 92, No. C7, 6933-6941.

Arola, A., 1999. Parameterization of turbulent and Mesoscale Fluxes for Heterogeneous Surfaces. J. of the Atmosph. Sciences, Vol. 56, No. 1-4, 584-598.

Beljaars, A. C. M.: 1994. The parameterization of surface fluxes in large scale models under free convection. Quart. J. Roy. Meteor. Soc., Vol. 121, 255-270.

Bergström, S., Carlsson, B., 1994. River runoff to the Baltic Sea: 1950-1990. Ambio 23 (4-5), 280-287.

Brümmer, B., Müller, G. Schröder, D. Kirchgäßner, A. Launianen, J. and Vihma, T.,2003. The eight BALTIMOS Field Experiments 1998-2001 over the Baltic Sea. Intern. BALTEX Secretariat Pub. No. 24, ISSN 1681-6471.

Brümmer, B., D. Schröder, J. Launiainen, T. Vihma, A. Smedman, and M. Magnusson, 2002. Temporal and spatial variability of surface fluxes over the ice edge zone in the northern Baltic Sea. J. Geophys. Res., Vol. 107, No. C8, 3096.

Burling, R. W., Stewart, R. W., 1967. Ocean-Atmosphere Interaction (microprocesses). Encyclopedia of Oceanography, Fairbridge, R. (Ed.), Rheinholdt, 571-576.

Calanca, P., 2001. A note on the roughness length for temperature over ,melting snow and ice. Q. J. R. Meteor. Soc. Vol. 127, 255-260.

Carlsson, M., 1998. Mean sea-level topography in the Baltic Sea determined by oceanographic methods. Marine Geodesy 21 (3), 203-217.

Cheng, Y., Vihma, T., 2002. Idealized study of a 2-D coupled sea-ice/atmosphere model during warm air advection. J. Glaciol., 48, 425-438.

DeCosmo, J., Katsaros, K. B., Smith, S. D., Anderson, R. J., Gost, W. A., Bunike, K., Chadwick, H., 1996. Air-sea exchange of water vapor and sensible heat: The HEXOS results. J. Geophys. Res.,

Vol. 101, No. C5, 12001-12016.

Ekman, M., 1996. A common pattern for interannual and periodical sea-level variations in the Baltic Sea and adjacent waters. Geophysica, Finnish Geophysical Society, Helsinki 32 (3), 261-272.

Ekman, M., Mäkinen, J., 1996. Mean sea surface topography in the Baltic Sea and its transition area to the North Sea: A geodetic solution and comparisons with oceanographic models. Journal of Geophysical Research, Vol. 101, No. C5, 11993-11999.

Hagedorn, R., 2000. Ein gekoppeltes Atmosphäre-Ozean-Modell für das Ostsee-Einzugsgebiet. Dissertation, Christian-Albrechts-Universität Kiel.

Hagedorn, R., Lehmann, A., Jacob, D., 2000. A coupled high resolution atmosphere-ocean model for the BALTEX region. Meteorol. Z., 9, 1, 7-20.

Joffre, S. M., 1982. Momentum and heat transfers in the surface layer over a frozen sea. Bound. Layer Meteor., Vol. 24, 211-229.

Johansson, C., Smedman, A.-S., Högström, U., Brasseur, J. G., Khanna, S., 2001. Critical Test of the Validity of Monin-Obukhov Similarity during Convective Conditions. J. of the Atmosph. Sciences, Vol. 58, No. 10-12, 1549-1566.

Kankaanpää, P., 1988. Morphology of a Baltic Sea ice pressure ridge. Geophysica , No. 24 (1-2), 15–33.

Krauss, W. 1981. The erosion of the thermocline. J. of Phys. Oceanography, Vol. 11, 415-433.

Large, W. G., Pond, S., 1981. Open ocean momentum flux measurements in moderate to strong winds. J. of Phys. Oceanography, Vol. 11, 324-336.

Large, W. G., Pond, S., 1982. Sensible and latent heat flux measurements over the ocean. J. of Phys. Oceanography, Vol. 12, 464-482.

Launiainen, J., Vihma, T., 1990. Derivation of turbulent surface fluxes-An iterative flux-profile method allowing arbitrary observing heights. Environ. Software. 5, 113-124.

Lehmann, A., 1995. A three-dimensional baroclinic eddy-resolving model of the Baltic Sea. Tellus 47, 1013-1031.

Lehmann, A., Hinrichsen, H.-H., 2000a. On the thermohaline variability of the Baltic Sea. J. Mar. Sys. 25, 333-357.

Lehmann, A., Hinrichsen, H.-H., 2000b. On the wind driven and thermohaline circulation of the Baltic Sea. Phys. Chem. Earth (B) 25(2), 183-189.

Lehmann, A., Hinrichsen, H.-H., 2002. Water, heat and salt exchange between the deep basins of the Baltic Sea. Boreal Environmental Res., 7, 405-415.

Lehmann, A., Krauss, W., Hinrichsen, H.-H., 2002. Effects of remote and local atmospheric forcing on circulation and upwelling in the Baltic Sea. Tellus, 54 A, 299-316.

Leppäranta, M., Hakala, R., 1992. The structure and strength of first-year ice ridges in the Baltic Sea. Cold Region Science and Technology, No. 20, 295–311.

Lundin, M., Håkansson, B., 2000. Time series analysis of sar sea ice backscatter. In Proceeding of a Whorkshop on Mapping and Archiving of Sea Ice Data - the Expanding Role of Radar, 329–334.

Makin, V. K., 1998. Air-sea exchange of heat in the presence of wind waves and spray. J. Geophys. Res., Vol. 103, No. C1, 1137-1152.

McPhee, M. G., 1992. Turbulent heat flux in the upper ocean under sea ice. J. Geophys. Res., Vol. 97, No. C4, 5365-5379.

Oke, T. R., 1978. Boundary layer climates. Methuen & Co. Ltd., London

Omstedt, A., 2001. Modelling the Bothnian Bay water and heat balance: the BALTEX-BASIS experiment. Launiainen, J., Vihma, T. (Eds.), BALTEX-BASIS Final Report, International BALTEX Secretariat, Publication No. 19.

Omstedt, A., Rutgersson, A., 2000. Closing the water and heat cycles of the Baltic Sea. Meteorol. Z., No. 9, 57-64.

Omstedt, A., Elken, J., Lehmann, A., Piechura, J., 2004. Knowledge of the Baltic Sea physics gained during the BALTEX and related programmes. Progress in Oceanography, 63, 1-28.

Palosuo, E., 1961. Crystal structure of brackish and freshwater ice. IASH, (54), 9-14.

Paulson, C. A., 1970. Representation of wind speed and temperature profiles in the unstable atmospheric surface layer. J. Appl. Meteor., Vol. 9, 857-861.

Rascke, E. et al., 2001. The Baltic Sea Experiment (BALTEX): A European Contribution to the Investigation of the Energy and Water Cycle over a Large Drainage Basin. Bulletin of the American Meteorological Society Vol. 82, No. 11, 2389–2413.

Rheinheimer, G., 1996. Meereskunde der Ostsee. Springer-Verlag Berlin Heidelberg New York, 2. Auflage.

Rutgersson, A., Smedman, A.-S., Omstedt, A., 2001. Measured and simulated latent and sensible heat fluxes at two marine sites in the Baltic Sea. Bound.- Layer Meteorol., Vol. 99, 53-84.

Samuelsson, M. and Stigebrandt, A., 1996. Main characteristics of the long-term sea level variability in the Baltic Sea. Tellus, 48 A (5), 672-683.

Schinke, H., Matthäus, W., 1998. On the cuases of major Baltic inflows an analysis of long time series. Cont. Shelf Res., 18, 67-97.

Schmidt, G. A., Bitz, C. M., Mikolajewicz, U., Tremblay, L. B., 2004. Ice-ocean boundary conditions for coupled models. Ocean Modelling, 7, 59-74.

Schröder, D., Vihma, T., Kerber, A., Brümmer, B., 2003. On the parameterization of turbulent surface fluxes over heterogeneous sea ice surfaces. J. Geophys. Res., Vol. 108, No. C6, 3195.

Seinä, A., Peltola, J., 1991. Jäätalven kestoaika ja kiintojään paksuustilastoja merialueilla 1961-1990 / Duration of the ice season and statistics of fast ice thickness along the Finnish coast 1961-1990. Finnish Marine Research, No 258.

Shirasawa, K. K., Kobinata, K., Kawamura, T., 2001. Eddy flux measurements below ice and oceanic boundary layer studies. Launiainen, J., Vihma, T. (Eds.), BALTEX-BASIS Final Report, International BALTEX Secretariat, Publication No. 19

Smedman, A.-S., Högström, U., 2000. What have we learnt from the field experiments? Gustafsson, N. (Ed.), BALTEX Baltic Sea Experiment, International BALTEX Secretariat, Publication No. 17

Smith, S. D., 1988. Coefficients for sea surface wind stress, heat flux, and wind profiles as a function for wind speed and temperature. J. Geophys. Res., Vol. 93, No. C12, 15467-15472.

Smith, S. D., 1989. Water vapor flux at the sea surface. Bound. Layer Meteor., Vol. 47, 277-293.

Smith, S. D., Fairall, C. W., Geernaert, G.L., Hasse, L., 1996. Air-sea fluxes: 25 years of progress. Bound.-Layer Meteorol., Vol. 78 (3-4), 247-290.

Smith, S. D., Muench, R. D., Pease, C. H., 1990. Polynyas and Leads: an Overview of Physical Processes and Environment. J. Geophys. Res., Vol. 95, No. C6, 9461-9479.

Stewart, R. H., 2005. Introduction to physical oceanography. Department of Oceanography. Texas A&M University.

Samuelsson, M., Stigebrandt, A., 1996. Main characteristics of the long-term sea level variability in the Baltic Sea. Tellus, Vil. 48A(5), 672-683.

Stigebrandt, A., 2001. Physical Oceanography of the Baltic Sea, Ch. 2. In: A Systems Analysis of the Baltic Sea (eds F. Wulff, L. Rahm and P. Larsson). Springer-Verlag, Berlin.

Stössel, A., Owens, W.B., 1992. The Hamburg sea-ice model. DKRZ Techn. Rep. No. 3.

Stull, R. B., 1988. An Introduction to Boundary Layer Meteorology. Kluwer Academic Publications.

Vihma, T., 2005. Modelling of the atmospheric boundary layer over sea ice. HIRLAM newsletter 48.

Vihma, T., Brümmer, B., 2002. Observations on modelling of on-ice and off-ice flows in the northern Baltic Sea. Bound.-Layer Meteorol., Vol. 103, 1-27.

Vihma, T., Haapala, J., 2005. Sea Ice. Progress in Oceanography, submitted.

Wyrtki, K. 1953/1954. Die Dynamik der Wasserbewegungen im Fehmarnbelt I und II. Kieler Meeresforsch., Vol. IX, 155-170; Vol. X, 162-181.

Acknowledgements

I would like to thank Dr. Andreas Lehmann for his support, patience and the pleasant climate during this work, further for the scientific suggestions and assistance in programming and the English language. Without him my knowledge about the Baltic Sea and the physics of the ocean would mostly be concealed for me. Thanks!

I am grateful to Burghard Brümmer and Amelie Kirchgäßner, who provided the data of the BALTIMOS field experiments and Frauke Nevoigt who provided weather data of our institute and Kiel lighthouse. Satellite SST data were kindly provided by the Bundesamt für Seeschiffahrt und Hydrographie in Hamburg, Germany.

Many thanks goes to my friends Kerstin Schepanski, Uta Neumann and Claudia Denker for the nice time during the study, the help and support as well as the many constructive and interesting discussions.
For the impulse, the assistance and the full of prevations time I would like to thank Dirk Schwerdtfeger.
And a whole affectionate thank to my family and my guardian angels.

Erklärung

Hiermit bestätige ich, dass ich die vorliegende Diplomarbeit selbständig verfasst und keine anderen als die angegebenen Quellen und Hilfsmittel verwendet habe.

Ich versichere, dass diese Arbeit noch nicht zur Erlangung eines Diplomgrades an anderer Stelle vorgelegen hat.

Kiel, September 2006

(Claudia Rudolph)